HANDBOOK OF ROBOTIC AND IMAGE-GUIDED SURGERY



ELSEVIER

Handbook of Robotic and Image-Guided Surgery

Handbook of Robotic and Image-Guided Surgery

Edited by

Mohammad H. Abedin-Nasab
Rowan University, Glassboro, New Jersey, United States
Robossis, Glassboro, New Jersey, United States

ELSEVIER

Elsevier
Radarweg 29, PO Box 211, 1000 AE Amsterdam, Netherlands
The Boulevard, Langford Lane, Kidlington, Oxford OX5 1GB, United Kingdom
50 Hampshire Street, 5th Floor, Cambridge, MA 02139, United States

Notices

Knowledge and best practice in this field are constantly changing. As new research and experience broaden our understanding, changes in research methods, professional practices, or medical treatment may become necessary.

Practitioners and researchers must always rely on their own experience and knowledge in evaluating and using any information, methods, compounds, or experiments described herein. In using such information or methods they should be mindful of their own safety and the safety of others, including parties for whom they have a professional responsibility.

To the fullest extent of the law, neither the Publisher nor the authors, contributors, or editors, assume any liability for any injury and/or damage to persons or property as a matter of products liability, negligence or otherwise, or from any use or operation of any methods, products, instructions, or ideas contained in the material herein.

British Library Cataloguing-in-Publication Data
A catalogue record for this book is available from the British Library

Library of Congress Cataloging-in-Publication Data
A catalog record for this book is available from the Library of Congress

ISBN: 978-0-12-814245-5

Publisher: Mara Conner
Acquisition Editor: Fiona Geraghty
Editorial Project Manager: Joshua Mearns
Production Project Manager: Sruthi Satheesh
Cover Designer: Mark Rogers

Typeset by MPS Limited, Chennai, India

Dedication

To my parents;
my wife;
and
my children.

About the Book

Handbook of Robotic and Image-Guided Surgery provides state-of-the-art systems and methods for robotic and computer-assisted surgeries. In this masterpiece, contributions from 169 researchers from 19 countries have been gathered to provide 38 chapters. This handbook consists of over 744 pages, including 659 figures and 61 videos.

It also provides basic medical knowledge for engineers and basic engineering principles for surgeons. A key strength of this text is the fusion of engineering, radiology, and surgical principles into one book, as follows:

- a thorough and in-depth handbook on surgical robotics and image-guided surgery which includes both fundamentals and advances in the field;
- a comprehensive reference on robot-assisted laparoscopic, orthopedic, and head-and-neck surgeries;
- chapters are contributed by worldwide experts from both engineering and surgical backgrounds.

Handbook of Robotic and Image-Guided Surgery

Mohammad H. Abedin-Nasab, Editor

38 CHAPTERS
744 PAGES

169 AUTHORS

68 INSTITUTIONS:

33 UNIVERSITIES
22 HOSPITALS
13 COMPANIES

19 COUNTRIES

61 VIDEOS
3 H 30 MIN

659 FIGURES

ELSEVIER

Foreword

LINK TO VIDEO

Russell H. Taylor
Johns Hopkins University, Baltimore, MD, United States

Computer-integrated systems are beginning to have an impact on surgical care comparable to that of computer-integrated systems in other sectors of our society. By combining human judgment with the capabilities of robotic and imaging technology and computer information processing, these systems can transcend human limitations to improve the precision, safety, and consistency of surgical interventions, while reducing their invasiveness. In addition to enabling better care for each individual patient, these systems enable the use of statistical methods combining information from many interventions to improve treatment processes for future patients.

The chapters of this book provide an excellent sampling of the current state-of-the-art in this rapidly developing field. When I was asked to write this foreword, I found myself wondering what to say. Upon reflection, I have decided to discuss a few general themes that have emerged over the 30 or so years that I have been working in this area and to speculate a little about what a similar collection produced some years from now might look like.

I first became aware of surgical robotics in 1985, at about the time of the first use of a robot in a stereotactic brain procedure [1], when IBM Research was approached by surgeons from the University of California at Davis to see if we could develop a robot for joint replacement surgery. This led to the development of the prototype of what was eventually commercialized by Integrated Surgical Systems (now Think Surgical) as the ROBODOC system [2–4]. Concurrently, we also developed a prototype computer-integrated planning and navigation system for craniofacial osteotomies with Court Cutting at NYU Medical Center [5,6]. One key attribute of these systems was that they combined steps of image-based modeling of the patient, use of the model to plan the intervention, registration of the model and plan to the patient, and the use of technology (robots, navigational trackers, video displays) to assist the surgeon in carrying out the procedure. Since much of my previous work had been in robotics for manufacturing, it seemed natural to refer to this process as surgical Computer-Aided Design (CAD)/Computer-Aided Manufacturing (CAM). Of course, there has been much progress over the past 30 years in these areas, and many of the systems reported in this book can reasonably be called surgical CAD/CAM systems.

In early 1991, I gave a talk at a SAGES meeting in Monterrey, CA. This was about the time that laparoscopic surgery was rapidly displacing conventional open surgery, and I began to wonder whether robotic systems could help surgeons address some of the associated technical problems. Several other researchers (notably, Satava [7,8], Green [9] and Wang [10]) had the same insight, and this work led to the development of several early commercial telerobotic laparoscopic surgery systems [10–13]. Work at IBM focused on a system we called the "LARS" [14,15], which combined teleoperation with image guidance and stereotactic applications. Although the LARS was never commercialized, many of its features (notably, the "remote center-of-motion" design and user interface concepts) have been widely adapted. These systems emphasize the interactive nature of surgical decision-making, and it is natural to think of them as surgical assistant systems. Again, many examples of such systems may be found in the chapters of this book.

I should emphasize that the distinction between surgical CAD/CAM and surgical assistant systems is both fuzzy and arbitrary. We are really dealing with systems that enable a three-way partnership between physicians, technology, and computers to improve surgical care. Accordingly, it is perhaps better to refer to the field as computer-integrated surgery or computer-integrated interventional medicine.

One very interesting aspect of this volume is an "organ directory" illustrating the rather broad scope of clinical application that the systems reported here address. As I mentioned earlier, the chapters in this collection provide an excellent sampling of current work in this field. It is necessarily a sampling. One could easily double (or even triple) the number of chapters in attempting to provide a truly complete coverage of current work. Given the very rapid progress in the field, truly comprehensive coverage will become even harder in the future.

However, I believe that some trends are emerging, and it may be useful to speculate about trends that may be found in some future *Encyclopedia of Computer-Integrated Surgery*. The organ directory will expand to cover essentially every part of the body, with structures at every scale, down to cellular levels. Technology will continue to advance to improve the dexterity and precision of robotic devices, which will be available in smaller and smaller scales to facilitate access inside the body. Imaging and other sensors will become increasingly integrated with tools, in order to provide direct feedback on tool-to-tissue interactions. Human−machine interfaces will continue to advance in order to improve ergonomics and to provide effective two-way communication between the physician and the system, in order to provide truly immersive environments for intraoperative decision-making and shared control.

However, I think that the biggest changes will be in the use of information at all phases of the treatment cycle. Advances in this area are, of course, highly synergistic with advances in technology and human−machine interfaces. One theme will be real-time information fusion to provide comprehensive, intraoperative modeling of the patient state. Other themes may be found in the emerging discipline of surgical data science [16], including the use of statistical modeling and machine learning to relate clinical outcomes to surgical technical outcomes, together with the use of these methods for treatment planning, decision support, and training.

Another theme will be increasing levels of "autonomy" exhibited by surgical robots. In many ways, robotic systems have always exhibited some level of autonomy, in the sense that computers convert surgeon intentions into motor control signals. Further, radiation machine therapy systems are arguably the first "surgical robots" and are highly autonomous surgical CAD/CAM systems; and systems like ROBODOC execute preplanned tool path trajectories to prepare bones to receive implants. There have recently been several attempts (e.g., Ref. [17]) to categorize levels of autonomy for surgical robots. These can provide useful insights, and there will certainly be systems exhibiting autonomy to varying degrees. As with the distinction between surgical CAD/CAM and surgical assistance, one need not get too hung up in drawing very fine distinctions. The key issues are: (1) unambiguously expressing the surgeon's intention for what the robot is to do; and (2) executing the intended commands with great reliability and safety.

To conclude, this book reflects something of a way point in the evolution of surgical technology from hand tools whose manipulation relies almost exclusively on a surgeon's own senses, memory, and appreciation of the patient state to a three-way partnership between surgeons, technology, and information to enhance clinical care. In exploring it, you may find it interesting and useful to consider how the systems reported reflect these broader themes and where future systems may build upon them.

References

[1] Kwoh YS, Hou J, Jonckheere EA, et al. A robot with improved absolute positioning accuracy for CT guided stereotactic brain surgery. IEEE Trans Biomed Eng 1988;35-2:153−61.

[2] Taylor RH, Paul HA, Kazanzides P, Mittelstadt BD, Hanson W, Zuhars JF, et al. An image-directed robotic system for precise orthopaedic surgery. IEEE Trans Robot Autom 1994;10-3:261−75.

[3] Bargar W, DiGioia A, Turner R, Taylor J, McCarthy J, Mears D. Robodoc multi-center trial: an interim report. In: Proc. 2nd Int. Symp. on medical robotics and computer assisted surgery, Baltimore, MD, November 4−7, 1995. p. 208−14.

[4] "Think Surgical", <https://thinksurgical.com>; 2018.

[5] Taylor RH, Paul HA, Cutting CB, Mittelstadt B, Hanson W, Kazanzides P, et al. Augmentation of human precision in computer-integrated surgery. Innov Technol Biol Med 1992;13-4:450−9 (special issue on computer assisted surgery).

[6] Cutting CB, Bookstein FL, Taylor RH. Applications of simulation, morphometrics and robotics in craniofacial surgery. In: Taylor RH, Lavallee S, Burdea G, Mosges R, editors. Computer-integrated surgery. Cambridge, MA: MIT Press; 1996. p. 641−62.

[7] Satava R. Robotics, telepresence, and virtual reality: a critical analysis of the future of surgery. Minim Invasive Ther 1992;1-:357−63.

[8] Satava RM. Surgical robotics: the early chronicles, a personal historical perspective. Surg Laparosc Endosc Percutan Tech 2002;12-1:6−16.

[9] Green P, Satava R, Hill J, Simon I. Telepresence: advanced teleoperator technology for minimally invasive surgery (abstract). Surg Endosc 1992;6-91.

[10] Sackier JM, Wang Y. Robotically assisted laparoscopic surgery. From concept to development. Surg Endosc 1994;8-1:63−6. Available from: http://www.ncbi.nlm.nih.gov/entrez/query.fcgi?cmd = Retrieve&d-b = PubMed&dopt = Citation&list_uids = 8153867.

[11] Reichenspurner H, Demaino R, Mack M, Boehm D, Gulbins H, Detter C, et al. Use of the voice controlled and computer-assisted surgical system Zeus for endoscopic coronary artery surgery bypass grafting. J Thorac Cardiovasc Surg 1999;118(1):11−16.

[12] Yoshino I, Hashizume M, Shimada M, Tomikawa M, Tomiyasu M, Suemitsu R, et al. "Thoracoscopic thymomectomy with the da Vinci computer-enhanced surgical system". J Thorac Cardiovasc Surg 2001;122-4:783−5.

[13] Tewari A, Peabody J, Sarle R, Balakrishnan G, Hemal A, Shrivastava A, et al. Technique of da Vinci robot-assisted anatomic radical prostatectomy. Urology 2002;60-4:569−72.

[14] Taylor R, Funda J, LaRose D, Treat M. A telerobotic system for augmentation of endoscopic surgery. In: IEEE conference on engineering in medicine and biology, Paris, October, 1992. p. 1054−6.

[15] Taylor RH, Funda J, Eldridge B, Gruben K, LaRose D, Gomory S, et al. A telerobotic assistant for laparoscopic surgery. IEEE Eng Med Biol Mag 1995;14-:279−87.

[16] Maier-Hein L, Vedula SS, et al. Surgical data science for next-generation interventions. Nat Biomed Eng 2017;1:691−6.

[17] Yang G-Z, Cambias J, Cleary K, Daimler E, Drake J, Dupont PE, et al. Medical robotics—regulatory, ethical, and legal considerations for increasing levels of autonomy. Sci Robot 2017;2(4):eaam8638, Editorial. doi:10.1126/scirobotics.aam8638.

Foreword

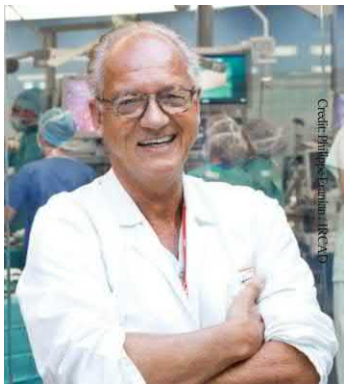

Jacques Marescaux[1,2,3]
[1]*University of Strasbourg, Strasbourg, France*
[2]*IHU Strasbourg, Strasbourg, France*
[3]*IRCAD, Strasbourg, France*

I am Professor of Surgery at the University of Strasbourg, Chairman of the Institute of Image-Guided Surgery (IHU Strasbourg), and President and Founder of the IRCAD (1994), a uniquely structured institute, dedicated to research and training, advancing the field of surgery into the information era. Over the last 24 years, this center has gained international acclaim by training more than 40,000 surgeons from 124 countries. In 2000, I developed WeBSurg, a virtual online surgical university resulting from the need to maintain the link between the training center and surgeons.

In 2001, I performed the first transcontinental laparoscopic surgery in a patient located in Strasbourg (France) while being in New York; this is known as "Operation Lindbergh" (*Nature* 2001). On April 2, 2007, I was the first in the world to operate, with my team, on a patient without leaving any scar (*Archives of Surgery* 2007).

Current telemanipulators have a common architecture made up of a command console, where the surgeon takes place. This console is equipped with haptic systems to remotely control the electromechanical instruments docked at the patient's side. End effectors replicate human movements.

In this configuration, the procedure should be properly defined as a computer-assisted surgery. The advantages of such an operating tool are multiple and immediately perceived, that is, enhanced ergonomics in the operating surgeon, enhanced stability of the camera system with, in most cases, 3D view, and precision movements, thanks to the filtering function which eliminates natural and physiological tremors. All these assets have been used collectively to generate a frankly undeniable marketing argument. Indeed, the telemanipulator enhances the skills of surgeons and shortens the learning curve of the minimally invasive surgery (MIS) approach radically. As a result, the sort of intelligence placed between the bare hand of the surgeon and the instruments has the potential to improve the uptake of MIS, for the benefit of a larger number of patients.

This is an apt argument. However, there are some drawbacks when it comes to the real-life application: current systems are expensive and entail extra costs associated with consumables, maintenance, increased operating room time for docking and undocking, and increased staffing needs.

If robotics will without a doubt allow the use of MIS for increasingly complex operations, there is so far no high level of evidence-based studies demonstrating a real benefit of "robotically" assisted MIS vs. standard MIS, as far as surgical outcomes and cost benefits are concerned.

This failure to demonstrate compelling advantages is easy to explain: the literature has been comparing robotic results with those of laparoscopic surgery performed in expert centers, however the main advantage of robotic surgery is to allow surgeons who do not necessarily have the required skills in conventional laparoscopic surgery to perform MIS.

Moreover, many new telemanipulators have been released, including flexible endoscopic platforms. While still in a master−slave configuration, the flexible endoscopic telemanipulator can outperform the standard systems when dealing with complex endoluminal surgery, including endoscopic submucosal dissections for early-stage cancer or per-oral endoscopic myotomy. A similar consideration can be applied to the field of percutaneous surgery, where energy-based tumor ablations can be greatly improved by electromechanical assistance and potentially reach comparable outcomes to surgical removal, in selected cases.

The future of real robotic surgery lies clearly in the development of completely autonomous and intelligent devices presenting context awareness with multiple sensors, artificial intelligence selecting the best theranostic algorithms, automatic task execution complemented with multimodal advanced imaging guidance, including virtual and augmented reality, fluorescence and hyperspectral imaging, and so on.

This groundbreaking product change, coupled with a think-out-of-the-box attitude in conceiving new processes and therapeutic approaches, will provide the real sense and potential of robotic technologies.

Companies which have developed commercially available telemanipulator systems should be credited for having opened the OR to mechatronics and for broadening surgeons' minds with these new and stimulating perspectives.

Within the next 5 years, many new "robots" will be released onto the market. This will facilitate healthy competition, and truly demonstrates that the change from conventional surgery to robotics is inevitable.

Dr. Abedin-Nasab should be congratulated for the great amount of work provided in bringing together 169 experts from 19 countries to create the *Handbook of Robotic and Image-Guided Surgery*. The handbook is an up-to-date, state-of-the-art of mechatronics applied to surgery, with great iconography and supplementary video material. The original chapter division based on engineering and clinical challenges facilitates the reading of the handbook. Future perspectives on the alternative use of telemanipulators are also nicely described. It is a fantastic achievement of a very demanding task.

About the Editor

Mohammad H. Abedin-Nasab specializes in surgical robotics, robotics, biomechanics, and nonlinear modeling. He has focused on both basic and applied research endeavors, ensuring that his research is consistently relevant to the scientific community as well as the health-care system and medical robotics industry. He has a passion for the development of novel technologies for application in critical areas of biomedicine, including clinical research and surgery.

Email: abedin@robossis.com

Acknowledgments

I thank God for all the blessings in my life.

I am grateful to Marziyeh Saeedi-Hosseiny for her great help and countless assistance on this project. I am sincerely thankful to Dr. Ali A. Houshmand, President of Rowan University, for his outstanding leadership and support for healthcare research. I am indebted to Dr. Arye Rosen, a member of the National Academy of Engineering and former Associate Vice President of Rowan University, for his unique support and guidance. Special thanks are due to Dr. Mark Byrne, Founding Head and Professor of the Department of Biomedical Engineering, Rowan University for his continuous help and invaluable advice.

I would like to express my sincere appreciation to Fiona Geraghty, Senior Acquisitions Editor at Elsevier, who was the key person at the publisher helping in the creation of this handbook. I am grateful to Kattie Washington, Serena Castelnovo, and Joshua Mearns who served as Editorial Project Managers of this project during a 2-year period. I would like to thank Sruthi Satheesh, Project Manager at Elsevier, and her team for their revisions and final touches to the handbook. My gratitude also goes to Mark Rogers who designed the very beautiful cover, and Matthew Limbert who designed impressively unique title pages for the chapters.

The chapters of this handbook have been thoroughly reviewed. I wish to express my heartfelt thanks for the care and thoughts of the reviewers; they are Riddhi Gandhi, Matthew Talarico, Manpreet Singh, Nicholas Silva, Matthew Goldner, Caroline Smith, Daniel Infusino, and Mason Weems.

Organs Directory

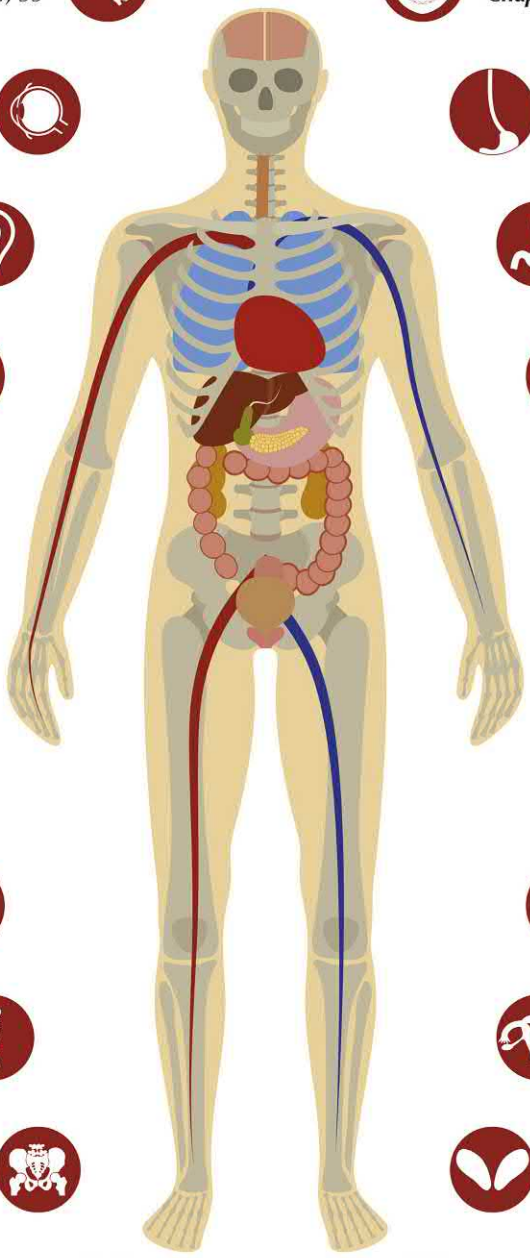

BRAIN
Chapters: *2, 15, 32, 33, 34, 35*

EYE
Chapter: *36*

EAR
Chapter: *37*

LUNG
Chapters: *1, 2, 3, 4, 5, 6, 7, 16, 17, 18*

BREAST
Chapters: *2, 22*

HEART
Chapters: *6, 15, 21*

CARDIOVASCULAR
Chapter: *20*

LONG BONE
Chapter: *30*

SPINE
Chapters: *2, 31, 32, 33*

PELVIS/HIP
Chapters: *1, 7, 23, 24, 31*

KNEE
Chapters: *23, 25, 26, 27, 28, 29, 31*

MOUTH & THROAT
Chapter: *38*

ESOPHAGUS
Chapter: *8*

STOMACH
Chapters: *1, 3, 4, 6, 7, 8,13, 16, 17, 18*

LIVER
Chapters: *2, 4, 5, 12, 13, 14, 15, 16, 18*

GALLBLADDER
Chapter: *5*

PANCREAS
Chapters: *3, 6*

KIDNEY
Chapters: *5, 14, 17*

BLADDER
Chapter: *6*

UTERUS
Chapters: *1, 3, 4, 5, 7, 15, 16, 17, 18*

PROSTATE
Chapters: *1, 2, 3, 4, 5, 7, 11, 15, 16, 17, 18, 19*

COLON
Chapters: *1, 3, 4, 6, 7, 8, 9, 10, 13, 15, 16, 17, 18, 19*

List of Contributors

Jake J. Abbott Department of Mechanical Engineering, University of Utah, Salt Lake City, UT, United States

Mohammad H. Abedin-Nasab Robossis, Glassboro, NJ, United States; Rowan University, Glassboro, NJ, United States

Ahmad Abiri University of California Los Angeles, Los Angeles, CA, United States

Elnaz Afshari Sina Robotics and Medical Innovators Co., Ltd., Tehran, Iran

Alireza Alamdar Sina Robotics and Medical Innovators Co., Ltd., Tehran, Iran; Sharif University of Technology, Tehran, Iran

Ali Alazmani University of Leeds, Leeds, United Kingdom

Oliver Anderson Colchester General Hospital, Colchester, United Kingdom

Axel Andres University of Geneva, Geneva, Switzerland

Maria Antico Queensland University of Technology, Brisbane, QLD, Australia

Tan Arulampalam Colchester General Hospital, Colchester, United Kingdom

Mahdi Azizian Intuitive Surgical, Sunnyvale, CA, United States

Christos Bergeles School of Biomedical Engineering and Imaging Sciences, King's College London, London, United Kingdom

Per Bergman Corindus Vascular Robotics, Waltham, MA, United States

James Bisley University of California Los Angeles, Los Angeles, CA, United States

Steven J. Blacker Corindus Vascular Robotics, Waltham, MA, United States

Andrea Boni University of Perugia, Perugia, Italy

Nicolas Christian Buchs University of Geneva, Geneva, Switzerland

Turgut Bora Cengiz Cleveland Clinic, Cleveland, OH, United States

Danny Tat-Ming Chan The Chinese University of Hong Kong, Hong Kong

Philip Wai Yan Chiu The Chinese University of Hong Kong, Shatin, Hong Kong

Hyouk Ryeol Choi Sungkyunkwan University, Suwon, South Korea

Darko Chudy Department of Neurosurgery, University Hospital Dubrava, Zagreb, Croatia; School of Medicine, Croatian Institute for Brain Research, University of Zagreb, Zagreb, Croatia

Giovanni Cochetti University of Perugia, Perugia, Italy

Ross Crawford Queensland University of Technology, Brisbane, QLD, Australia; Australian Centre for Robotic Vision, Brisbane, QLD, Australia; Prince Charles Hospital, Brisbane, QLD, Australia

William Cross St James's University Hospital, Leeds, United Kingdom

Peter Culmer University of Leeds, Leeds, United Kingdom

Simon Daimios Intuitive Surgical, Sunnyvale, CA, United States

Michel De Mathelin ICube Laboratory, Strasbourg, France

Elena De Momi Nearlab, Department of Electronics, Information and Bioengineering, Politecnico di Milano, Milan, Italy

Jacopo Adolfo Rossi De Vermandois University of Perugia, Perugia, Italy

Domagoj Dlaka Department of Neurosurgery, University Hospital Dubrava, Zagreb, Croatia

John R. Dooley Accuray, Sunnyvale, CA, United States

Luka Drobilo Faculty of Mechanical Engineering and Naval Architecture, UNIZAG FAMENA, University of Zagreb, Zagreb, Croatia

Erik Dutson University of California Los Angeles, Los Angeles, CA, United States

Thomas Erchinger Geisinger, Wilkes-Barre, Pennsylvania, United States

Zhencheng Fan Tsinghua University, Beijing, China

Richard Fanson Intellijoint Surgical, Waterloo, ON, Canada

Farzam Farahmand Sina Robotics and Medical Innovators Co., Ltd., Tehran, Iran; Sharif University of Technology, Tehran, Iran

Zahra Faraji-Dana 7D Surgical Inc., North York, ON, Canada

Koorosh Faridpooya Eye Hospital Rotterdam, Rotterdam, Netherlands

Anthony Fernando TransEnterix, Morrisville, NC, United States

Davide Fontanarosa Queensland University of Technology, Brisbane, QLD, Australia

Chee Wee Gan Department of Otolaryngology, National University of Singapore, Singapore, Singapore

Mathieu Garayt EOS Imaging, Paris, France

Gianluca Gaudio University of Perugia, Perugia, Italy

Emre Gorgun Cleveland Clinic, Cleveland, OH, United States

Jon C. Gould Medical College of Wisconsin, Milwaukee, WI, United States

Vincent Groenhuis Robotics and Mechatronics, University of Twente, Enschede, The Netherlands

Warren Grundfest University of California Los Angeles, Los Angeles, CA, United States

Ziyan Guo The University of Hong Kong, Hong Kong

Anjuli M. Gupta Geisinger, Wilkes-Barre, Pennsylvania, United States

Monika Hagen University of Geneva, Geneva, Switzerland

Rana M. Higgins Medical College of Wisconsin, Milwaukee, WI, United States

Andre Hladio Intellijoint Surgical, Waterloo, ON, Canada

Joe Hobeika EOS Imaging, Paris, France

Iulian Iordachita Department of Mechanical Engineering, Johns Hopkins University, Baltimore, MD, United States

Anjali Jaiprakash Queensland University of Technology, Brisbane, QLD, Australia; Australian Centre for Robotic Vision, Brisbane, QLD, Australia

Branislav Jaramaz Smith & Nephew, Pittsburgh, Pennsylvania, United States

David Jayne University of Leeds, Leeds, United Kingdom

Bojan Jerbić Faculty of Mechanical Engineering and Naval Architecture, UNIZAG FAMENA, University of Zagreb, Zagreb, Croatia

Alexander H. Jinnah Wake Forest School of Medicine, Winston-Salem, NC, United States

Riyaz H. Jinnah Southeastern Regional Medical Center, Lumberton, NC, United States; Wake Forest School of Medicine, Winston-Salem, NC, United States

Kelly R. Johnson Geisinger, Wilkes-Barre, Pennsylvania, United States

Yaqub Jonmohamadi Queensland University of Technology, Brisbane, QLD, Australia

Yen-Yi Juo University of California Los Angeles, Los Angeles, CA, United States

Marin Kajtazi Faculty of Mechanical Engineering and Naval Architecture, UNIZAG FAMENA, University of Zagreb, Zagreb, Croatia

Jin U. Kang Department of Electrical and Computer Engineering, Johns Hopkins University, Baltimore, MD, United States

John M. Keggi Orthopaedics New England, Middlebury, CT, United States; Connecticut Joint Replacement Institute, Hartford, CT, United States

Iman Khalaji Intuitive Surgical, Sunnyvale, CA, United States

Warren Kilby Accuray, Sunnyvale, CA, United States

Uikyum Kim Korea Institute of Machinery & Materials, Daejeon, South Korea

Yong Bum Kim Sungkyunkwan University, Suwon, South Korea

Sujith Konan University College London Hospitals, London, United Kingdom

Nicholas Kottenstette Corindus Vascular Robotics, Waltham, MA, United States

Ka-Wai Kwok The University of Hong Kong, Hong Kong

Ka Chun Lau The Chinese University of Hong Kong, Shatin, Hong Kong

Jeffrey M. Lawrence Gundersen Health System, Viroqua, WI, United States

Martin Chun-Wing Leong The University of Hong Kong, Hong Kong

Michael K.K. Leung 7D Surgical Inc., North York, ON, Canada

Yun Yee Leung The Chinese University of Hong Kong, Shatin, Hong Kong

Changsheng Li National University of Singapore, Singapore, Singapore

Wenyu Liang Department of Electrical and Computer Engineering, National University of Singapore, Singapore

Hongen Liao Tsinghua University, Beijing, China

Zhuxiu Liao Tsinghua University, Beijing, China

Chwee Ming Lim National University Hospital, Singapore, Singapore

Hsueh Yee Lim Department of Otolaryngology, National University of Singapore, Singapore, Singapore

May Liu Intuitive Surgical, Sunnyvale, CA, United States

Longfei Ma Tsinghua University, Beijing, China

Carla Maden University College London, London, United Kingdom

Michael J. Maggitti Southeastern Regional Medical Center, Lumberton, NC, United States

Adrian L.D. Mariampillai 7D Surgical Inc., North York, ON, Canada

Leonardo S. Mattos Biomedical Robotics Lab, Department of Advanced Robotics, Istituto Italiano di Tecnologia, Genoa, Italy

Calvin R. Maurer, Jr. Accuray, Sunnyvale, CA, United States

Ettore Mearini University of Perugia, Perugia, Italy

Jamie Milas EOS Imaging, Paris, France

Alireza Mirbagheri Tehran University of Medical Sciences, Tehran, Iran; Sina Robotics and Medical Innovators Co., Ltd., Tehran, Iran

Riddhit Mitra Smith & Nephew, Pittsburgh, Pennsylvania, United States

Sara Moccia Biomedical Robotics Lab, Department of Advanced Robotics, Istituto Italiano di Tecnologia, Genoa, Italy; Department of Information Engineering, Università Politecnica delle Marche, Ancona, Italy

Mehdi Moradi Sina Robotics and Medical Innovators Co., Ltd., Tehran, Iran

Philippe Morel University of Geneva, Geneva, Switzerland

George Moustris National Technical University of Athens, Athens, Greece

Jeffrey Muir Intellijoint Surgical, Waterloo, ON, Canada

Faisal Mushtaq University of Leeds, Leeds, United Kingdom

Florent Nageotte ICube Laboratory, Strasbourg, France

M. Ali Nasseri Ophthalmology Department, Technical University of Munich, Munich, Germany

Mohan Nathan TransEnterix, Morrisville, NC, United States

Michael Naylor Accuray, Sunnyvale, CA, United States

Gordian U. Ndubizu Geisinger, Wilkes-Barre, Pennsylvania, United States

Cailin Ng NUS Graduate School for Integrative Sciences and Engineering, Singapore, Singapore

Daniel Oh Intuitive Surgical, Sunnyvale, CA, United States

Yasushi Ohmura Department of Surgery, Okayama City Hospital, Okayama, Japan

Elena Oriot EOS Imaging, Paris, France

Ajay K. Pandey Queensland University of Technology, Brisbane, QLD, Australia; Australian Centre for Robotic Vision, Brisbane, QLD, Australia

Theodore Pappas Duke University School of Medicine, Durham, NC, United States

Andrea Peloso University of Geneva, Geneva, Switzerland

Jake Pensa University of California Los Angeles, Los Angeles, CA, United States

Veronica Penza Biomedical Robotics Lab, Department of Advanced Robotics, Istituto Italiano di Tecnologia, Genoa, Italy

Christopher Plaskos OMNI, Raynham, MA, United States

Wai-Sang Poon The Chinese University of Hong Kong, Hong Kong

Bogdan Protyniak Geisinger, Wilkes-Barre, Pennsylvania, United States

Liang Qiu National University of Singapore, Singapore, Singapore

Andrew Razjigaev Queensland University of Technology, Brisbane, QLD, Australia; Australian Centre for Robotic Vision, Brisbane, QLD, Australia

Hongliang Ren National University of Singapore, Singapore, Singapore

Cameron N. Riviere Robotics Institute, Carnegie Mellon University, Pittsburgh, PA, United States

Jonathan Roberts Queensland University of Technology, Brisbane, QLD, Australia; Australian Centre for Robotic Vision, Brisbane, QLD, Australia

Sheila Russo Boston University, Boston, MA, United States

Omid Saber Corindus Vascular Robotics, Waltham, MA, United States

Marzieh S. Saeedi-Hosseiny Robossis, Glassboro, NJ, United States; Rowan University, Glassboro, NJ, United States

Dominique Saragaglia CHU Grenoble-Alpes, South Teaching Hospital, Grenoble, France

Saeed Sarkar Tehran University of Medical Sciences, Tehran, Iran; Sina Robotics and Medical Innovators Co., Ltd., Tehran, Iran

Fumio Sasazawa Queensland University of Technology, Brisbane, QLD, Australia

Sohail Sayeh Accuray, Sunnyvale, CA, United States

Bojan Šekoranja Faculty of Mechanical Engineering and Naval Architecture, UNIZAG FAMENA, University of Zagreb, Zagreb, Croatia

William J. Sellers Geisinger, Wilkes-Barre, Pennsylvania, United States

Dong-Yeop Seok Sungkyunkwan University, Suwon, South Korea

Sami Shalhoub OMNI, Raynham, MA, United States

Françoise J. Siepel Robotics and Mechatronics, University of Twente, Enschede, The Netherlands

Saeed Sokhanvar Corindus Vascular Robotics, Waltham, MA, United States

Jonathan Sorger Intuitive Surgical, Sunnyvale, CA, United States

Beau A. Standish 7D Surgical Inc., North York, ON, Canada

Scott R. Steele Cleveland Clinic, Cleveland, OH, United States

Ivan Stiperski Faculty of Mechanical Engineering and Naval Architecture, UNIZAG FAMENA, University of Zagreb, Zagreb, Croatia

Stefano Stramigioli Robotics and Mechatronics, University of Twente, Enschede, The Netherlands; ITMO University, Saint Petersburg, Russia

Mario Strydom Queensland University of Technology, Brisbane, QLD, Australia

Hao Su City University of New York, New York City, NY, United States

Filip Šuligoj Faculty of Mechanical Engineering and Naval Architecture, UNIZAG FAMENA, University of Zagreb, Zagreb, Croatia

Songping Sun University of California Los Angeles, Los Angeles, CA, United States

Marko Švaco Faculty of Mechanical Engineering and Naval Architecture, UNIZAG FAMENA, University of Zagreb, Zagreb, Croatia

Raphael Sznitman ARTORG Center for Biomedical Engineering Research, University of Bern, Bern, Switzerland

Masahiro Takahashi Takahashi Surgery Clinic, Yamagata, Yamagata, Japan

Kok Kiong Tan Department of Electrical and Computer Engineering, National University of Singapore, Singapore

Anna Tao University of California Los Angeles, Los Angeles, CA, United States

Alex Todorov Cobot, United States

Christian Toso University of Geneva, Geneva, Switzerland

Morena Turco University of Perugia, Perugia, Italy

Marija Turković Faculty of Mechanical Engineering and Naval Architecture, UNIZAG FAMENA, University of Zagreb, Zagreb, Croatia

Costas Tzafestas National Technical University of Athens, Athens, Greece

Emmanuel Vander Poorten Department of Mechanical Engineering, KU Leuven, Heverlee, Belgium

Josip Vidaković Faculty of Mechanical Engineering and Naval Architecture, UNIZAG FAMENA, University of Zagreb, Zagreb, Croatia

Nikola Vitez Faculty of Mechanical Engineering and Naval Architecture, UNIZAG FAMENA, University of Zagreb, Zagreb, Croatia

Andrea Volpin Royal Derby Hospital, Derby, United Kingdom

Liao Wu Queensland University of Technology, Brisbane, QLD, Australia; Australian Centre for Robotic Vision, Brisbane, QLD, Australia

Yeung Yam The Chinese University of Hong Kong, Shatin, Hong Kong

Victor X.D. Yang Sunnybrook Health Sciences Centre, Toronto, ON, Canada

Philippe Zanne ICube Laboratory, Strasbourg, France

Adrian Žgaljić Faculty of Mechanical Engineering and Naval Architecture, UNIZAG FAMENA, University of Zagreb, Zagreb, Croatia

Xinran Zhang Tsinghua University, Beijing, China

Lucile Zorn ICube Laboratory, Strasbourg, France

Ivan Župančić Faculty of Mechanical Engineering and Naval Architecture, UNIZAG FAMENA, University of Zagreb, Zagreb, Croatia

1

Senhance Surgical System: Robotic-Assisted Digital Laparoscopy for Abdominal, Pelvic, and Thoracoscopic Procedures

Theodore Pappas[1], Anthony Fernando[2] and Mohan Nathan[2]

[1]*Duke University School of Medicine, Durham, NC, United States*
[2]*TransEnterix, Morrisville, NC, United States*

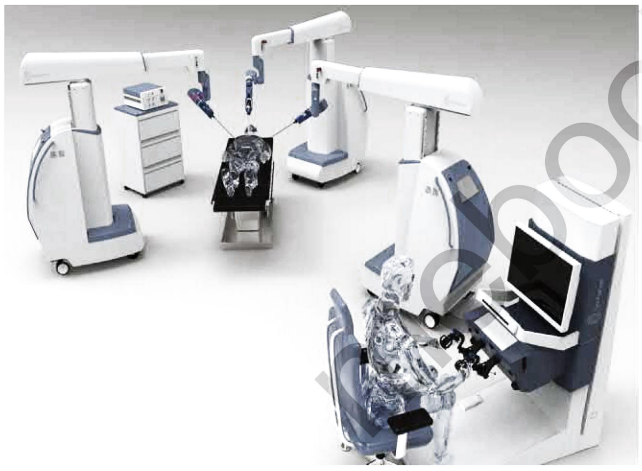

CHAPTER FOCUS
ENGINEERING & CLINICAL

TECHNOLOGY
ROBOTIC & IMAGE-GUIDED

LINK TO VIDEO

ABSTRACT

Robotic-assisted digital laparoscopy (Senhance Surgical System) provides a digitized interface between the surgeon and the patient designed to increase surgeon control and reduce surgical variability. The physical open architecture of the system is composed of independent robotic-assisted manipulator arms that are compatible with conventional trocars and familiar laparoscopic instruments—and thus taking advantage of the existing operating room and surgical suite ecosystem. The fully reusable nature of the Senhance instruments allows for no preset limitation to the number of reuses of the instruments. Instrument movement is precise, scaled, and tremor-free with haptic feedback and familiar laparoscopic motions and technique. Digital 3D imaging with eye tracking provides continuous camera control by the surgical operator. Surgeon and support staff training includes learning the operation of the system and leverages existing laparoscopic technique and equipment. Postoperative evaluation of the system is by postmarket registry. Clinical and cost outcomes are described and summarized. Digital laparoscopy leverages surgical expertise of general and gynecologic laparoscopic surgeons and is designed to increase surgeon control, reduce variability, improve efficiencies, and eliminate waste.

Handbook of Robotic and Image-Guided Surgery. DOI: https://doi.org/10.1016/B978-0-12-814245-5.00001-3

STOMACH LUNG PELVIS COLON UTERUS PROSTATE

1.1 Challenges of general surgery and the need for value-driven solutions

Traditional laparoscopy is the gold standard of minimally invasive surgery (MIS): it provides patients with improved perioperative outcomes, improved postoperative recovery with earlier return to normal activity and work, and minimal incisions and scarring compared to open surgery. Patients commonly are discharged the same day they undergo laparoscopic procedures—unlike the longer and increased care required for inpatients following open surgery. Although these benefits to patient outcomes of laparoscopic surgery are not debated, less has been reported on the physical and mental toll of laparoscopy on the general surgeon [1,2]. Park and colleagues revealed that 86.9% of laparoscopic surgeons suffer from performance-related symptoms, with the principal predictor being high case volume [1]. Burnout—a syndrome characterized by emotional exhaustion, depersonalization, and a decreased sense of personal accomplishment caused by work-related stress—is particularly prevalent in surgical specialties (with a range of 32%−55%) and has a 49% prevalence among general surgeons [3,4]. Considering the ergonomic, vision, and control limitations of laparoscopy, the high rate of general surgeon burnout, and our growing elderly patient population, healthcare systems need to adapt to the shifting technological environment and address and update technology to help surgeons do their jobs efficiently and effectively.

General surgeons operate across a broad range of surgical indications including those among a heterogeneous and growing elderly patient population, and the high burnout rate among general surgeons indicates they may not be able to keep up with patient demand. These factors feed surgical variability, which often leads to disparate outcomes for patients and higher resource utilization, costs, and waste, such as time, inventory, motion, waiting, and skills. Value-based healthcare requires hospitals to find new ways to deliver the best clinical outcome relative to the optimal cost of care within an environment that fosters the right patient experience delivered by engaged and satisfied surgeons.

Until recently, innovations have not been driven to benefit all stakeholders—patients, surgeons, hospitals, and government and private payers—and have not addressed operating room inefficiencies, cost containment, and surgical variability. Current technology does not leverage existing laparoscopic experience and training and, as a result, imposes a high hurdle to learning new techniques.

Robotic-assisted digital laparoscopy with the Senhance Surgical System (TransEnterix, Inc., Morrisville, NC, United States) (formerly Telelap Alf-X; SOFAR, Milan, Italy) is designed to be used in the majority of laparoscopic procedures, with similar operating room times to laparoscopy and comparable per-procedure costs to standard laparoscopy. The fully reusable nature of the Senhance instruments allows for no preset limitation to the number of reuses of the instruments. The only true disposable component of the system is the required sterile draping. The 3D digitized interface between the surgeon and the patient affords surgeon control and reduces surgical variability. The open architecture system comprises independent robotic-assisted manipulator arms that are compatible with conventional trocars and familiar instruments—thereby, leveraging the existing operating room and surgical suite environment. Senhance builds on the foundation of laparoscopy and is powered by robotic features, such as haptic feedback and eye tracking, which facilitate the transition to robotic-assisted digital laparoscopic procedures by laparoscopic surgeons.

In the following pages, we describe the engineering and technological premises of robotic-assisted digital laparoscopy, detail the flow of surgical training and procedure planning, define the benefits and value to patients, providers, hospitals, and payers, and describe associated clinical and costs outcomes.

1.2 Robotic-assisted digital laparoscopy

Robotic-assisted digital laparoscopy with the Senhance Surgical System is best described as a digitized interface between the surgeon and the patient during a laparoscopic procedure that enhances surgeon control of the instruments. From an ergonomically supportive open console, the surgeon controls visualization of the surgical field and senses haptic forces of the instrument−tissue interface. Eye-tracking visualization allows the surgeon continuous control of the camera without needing to interrupt performing the procedure to reposition the camera or rely on support staff to adjust the laparoscope's field of view. The sensation of touch and force was designed into the system to minimize tissue trauma. The force sensing not only provides feedback to the surgeon, it alerts the surgeon if excessive force is detected either at the instrument or the abdominal wall. Regardless of their laparoscopic experience or their engagement with the system's force feedback, surgeons rapidly adapt to the controls of Senhance [5]. The robotic component allows minimally invasive access to difficult-to-reach anatomy; precise, scaled, and tremor-free instrument control; and the ability to visualize within anatomically tight spaces using 3D cameras. The latter confers clarity of detail regarding delicate tissues and depth and spatial relationships in the surgical field.

1.2.1 System components

Senhance is an open-architecture, console-based, multiarm surgical system that enables a surgeon to control surgical instrumentation remotely during MIS in the lower abdomen, pelvis, and thoracic cavity. The capital equipment is comprised of three main subsystems (Fig. 1.1):

- *Console*: The station where the surgeon inputs information through hand and eye movements to direct the motion of the arms in the surgical field.
- *Manipulator arms*: Independent mechanized support arms that interface with the endoscope and surgical instruments. The manipulator arms produce output movements based on the instructions from the surgeon at the console. The system is configurable with up to three arms in the United States and up to four arms in the European Union.
- *Node*: A relay unit which connects the console inputs to the manipulator arms in the system and which converts and transmits the video signals to the 2D/3D monitor on the console.

The open architecture benefits the surgeon, patient, hospital, and payer. The system's compatibility with conventional surgical tools (Table 1.1) not only reduces the hospital's capital investment in system-specific equipment, it leverages the surgeon's and surgical team's familiarity with conventional laparoscopic equipment and makes possible rapid, as-needed conversion to standard laparoscopic or hybrid procedures.

With the open console, the surgeon can maintain a comfortable seating posture and view the entire operating room as well as make use of the eye-tracking software to move the laparoscope for constant imaging and assessment of the surgical field as well as to manipulate the instruments. This smooth and continuous camera control reduces the surgeon's reliance on additional support staff to manually move the laparoscope.

The optimal turning and pivot point of each trocar is calculated within each manipulator arm so as to minimize bruising and trauma to the port site tissue. Each arm is linked electronically to the node, which processes data regarding the positioning of each arm and the connected instrument and its degrees of movement. The output is transmitted to the console, the console monitor, and an operating room monitor. The operating room monitor transmits the same operating field view to the surgical assistant and nurse.

Laparoscopic techniques and approaches are the foundation of the system. As indicated in Table 1.1, Senhance procedures integrate standard trocars, which allow the surgical assistant to intervene laparoscopically if needed and to use additional standard instruments through other ports. In addition, the console, manipulator arms, and node are in close proximity to the patient, which permits quick transition from the console to the patient in the event the surgeon decides to convert the procedure to standard laparoscopy or open surgery. The proximity of the surgeon console to the patient also facilitates verbal communication within the team. Lastly, the entirety of the system can be installed in a standard operating theater and, consequently, does not require creation of a dedicated space.

FIGURE 1.1 Typical operating room setup with the Senhance Surgical System. The console is in the foreground with the patient table in the middle of the image with the manipulator arms, laparoscope, and instruments in place. A secondary monitor, which shows the same view of the operative field that the surgeon sees, is available to the assistant and nurse.

TABLE 1.1 Surgical equipment compatible with the Senhance Surgical System.

Category	Equipment manufacturer and instrument family
Camera and vision	CONMED 3DHD
	NOVADAQ PINPOINT
	Stryker 1588 AIM
	Richard Wolf 3DHD[a]
Electrosurgical	CONMED System 5000
	Covidien/Valleylab ForceTriad
	Covidien/Valleylab Force FX
	Erbe VIO 300D
	BOWA ARC 400[a]
Patient table	Any operating table used for laparoscopic surgery
Insufflator	Any insufflator used for laparoscopic surgery
Trocar	Any trocar used for laparoscopic surgery
Suction irrigation	Any suction irrigation unit used for laparoscopic surgery

[a]*Available only in CE-marked countries.*

FIGURE 1.2 Typical Senhance setup that includes three manipulator arms for a supine patient. *Credit: © 2018 TransEnterix, Inc.*

1.2.1.1 Patient positioning

The surgeon can position the patient according to the requirements of the procedure and the patient's medical condition. Most laparoscopic procedures are performed with the patient supine and often in a Trendelenburg or reverse Trendelenburg position, depending on the anatomical location of the surgery (lower pelvis or foregut, respectively). Because the robotic manipulator arms are independent from one another, the surgeon can position the patient prior to surgery, as well as change the patient's position during the case, without requiring disconnection of the arms from the patient. The independence and mobility of each arm confer positioning advantages over stationary, single-unit robotic-assisted devices. Three-arm setups of the system with the patient supine or lateral are presented in Figs. 1.2 and 1.3, respectively.

Certain procedures, such as partial or total nephrectomy, adrenalectomy, pulmonary lobectomy, and thymectomy, are best performed with the patient on his or her side to facilitate access to the targeted anatomy. The system does not impose restrictions on optimal patient positioning.

A four-arm setup for a supine patient is presented in Fig. 1.4.

FIGURE 1.3 Typical Senhance three-arm setup for a patient in the lateral position. *Credit: © 2018 TransEnterix, Inc.*

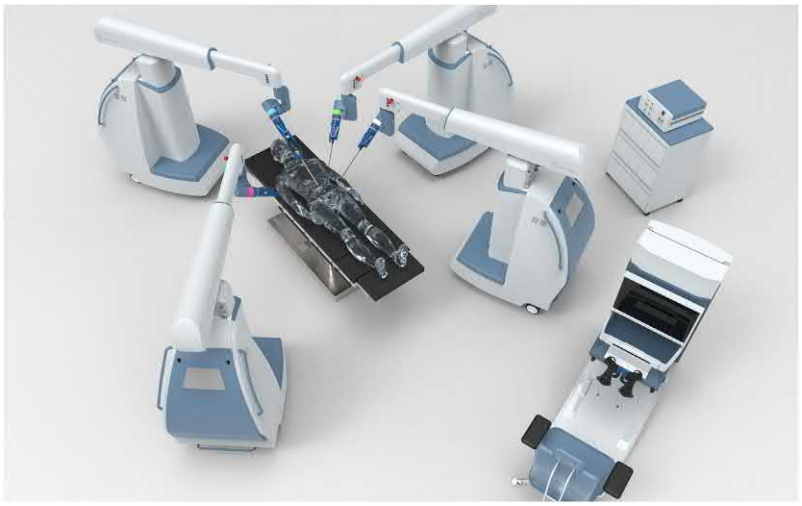

FIGURE 1.4 Senhance four-arm setup for a supine patient. *Credit: © 2018 TransEnterix, Inc.*

1.2.1.2 Docking

The docking time is the period required to adjust all settings, and determine and set the optimal positions of the robotic arms and intraabdominal placement of the instruments prior to starting the procedure. Stephan et al. recently reported their early experience with Senhance as applied to visceral surgery [6]. The majority of the procedures that these experienced laparoscopic surgeons performed were unilateral transabdominal preperitoneal (TAPP) inguinal hernia repairs and bilateral TAPP inguinal hernia repairs. As the surgeons became more adept with the system they advanced their efforts to more complicated procedures including cholecystectomy and sigmoid resection. During the first 5 months, they achieved an average docking time of $<$9 minutes and, for the last 20 procedures during that 5-month period, their average docking time was 7 minutes. Their docking times were similar to those reported by others who used the surgical system in gynecologic and colorectal surgery [7–15]. Stephan's average console time for the 29 cases of inguinal hernia repair was 37 minutes.

1.2.1.3 Eye sensing

Eye-sensing technology has been used for years to assist individuals who have cerebral palsy, quadriparesis, or other disabling physical and cognitive conditions that prevent the user from utilizing a traditional human–machine interface, such as a computer mouse or trackpad. Eye sensing or eye tracking determines where the user is looking at a screen by measuring reflections in the eye corneas; this process of controlling the computer through gazing at the screen is called gaze interaction. The system emits a near-infrared light at specific duty cycles, and the system computes the

gaze position and distance of the user after an initial calibration. The system's digital imaging and eye tracking are intended for use with current visualization technologies (Table 1.1) and take advantage of 2D and 3D high-definition laparoscopic imaging systems that are based on white light and 2D indocyanine green fluorescence imaging.

Senhance's eye-sensing system assists the surgeon in positioning the endoscope and the attached manipulator arm or navigating the functions area of the console monitor. The surgeon can also choose to use the trackpad and handles at the console to move the endoscope instead of taking advantage of eye sensing. The system first completes a calibration sequence, which includes verification that the surgeon's eye position can be read. Without successful calibration, the system turns off the eye tracker and the eye tracker cannot be overridden by the user.

Several safety mitigations are built into the eye-sensing system. The system only permits the surgeon to reposition the endoscope under the surgeon's control, which is accomplished after depressing the select button on both the right and left handles while the surgeon gazes at a position on the screen. The system then moves the endoscope in the direction of the surgeon's gaze. Motion is stopped when either of the two select buttons is released or when the gaze is lost—thus preventing unintended movement of a manipulator arm or surgical instrument.

1.2.1.4 Fulcrum

The console of the Senhance Surgical System includes two handles styled similarly to traditional laparoscopic handles; these console handles can command up to three or four manipulator arms. The manipulator arms connect to modified laparoscopic instruments (graspers, needle holders, scissors, etc.), which are used through trocars to grasp, dissect, mobilize, suture, and retract tissue in an insufflated abdominal space in the same manner as laparoscopy.

The end of each robotic manipulator arm is instrumented with force and torque sensors. These sensors determine the fulcrum point or the point of intended rotation of an inserted trocar. The sensors also prevent application of excessive force to surrounding tissue. During set up, a modified laparoscopic instrument is magnetically coupled with an adaptor to the manipulator arm and is inserted into the abdomen through a trocar. The arm makes very small movements to locate the center of rotation of the trocar, that is, the center of the incision point. Once this point has been captured in 3D space, the arm moves the instrument around and through the fulcrum point of the trocar to minimize stress to the surrounding tissue and to the incision site. As with standard laparoscopy, as the surgeon moves the instrument handle, the working tip or effector moves in the opposite direction; this paradoxical motion is conveyed on the console and operating room monitors.

1.2.1.5 Force feedback (haptics)

The scaled 1:1 force feedback feature of the Senhance System measures the forces experienced by the instruments in the *X*, *Y*, and *Z* Cartesian plane and transfers these forces electronically to the handles at the console. Accordingly, the surgeon receives and perceives the same forces that he or she experiences when using standard laparoscopic instrumentation for the same surgical maneuvers and with a high degree of sensitivity (35 g). Force feedback helps to ensure that the surgeon has seamless real-time access to relevant information about instrument tip−tissue contact. The surgeon perceives tissue presence, contact, and relative stiffness via force feedback information regarding contacted tissues with the instrument tips and/or shaft during surgical maneuvers. When combined with the depth of the palpation and instrument tip geometry information provided by the vision system, the user can perceive the physical characteristics of the tissue.

1.2.2 Indications

In the United States, the system is indicated for adult use and is intended to assist in the accurate control of laparoscopic instruments for visualization and endoscopic manipulation of tissue including grasping, cutting, blunt and sharp dissection, approximation, ligation, electrocautery, suturing, mobilization, and retraction in laparoscopic gynecological surgery, colorectal surgery, cholecystectomy, and inguinal hernia repair. In the European Union, Senhance has received the CE mark and is intended to be used in adults for laparoscopic surgery in the abdomen and pelvis and for limited uses in the thoracic cavity excluding the heart and greater vessels. Currently labeled US and EU procedures are listed in Table 1.2.

The system is contraindicated for use in surgeries where laparoscopic approaches and techniques are contraindicated. Currently available and fully reusable surgical instruments that are system-specific are listed in Table 1.3. Of

TABLE 1.2 Labeled procedures for the Senhance Surgical System in the United States and the European Union.

United States	European Union
Colorectal surgery	
Lower anterior resection including total mesorectal excision	Lower anterior resection including total mesorectal excision
Colectomy (right, left, total, transverse, hemicolectomy, sigmoidectomy)	Colectomy (right, left, total, transverse, hemicolectomy, sigmoidectomy)
Rectopexy	Rectopexy
Small bowel resection	Small bowel resection
Abdominoperineal resection	Abdominoperineal resection
Gynecological surgery	
Radical hysterectomy	Radical hysterectomy
Total hysterectomy	Total hysterectomy
Ovarian cystectomy	Ovarian cystectomy
Oophorectomy	Oophorectomy
Myomectomy	Myomectomy
Lymphadenectomy	Lymphadenectomy
Endometriosis resection	Endometriosis resection
Salpingectomy	Salpingectomy
Adnexectomy	Adnexectomy
Omentectomy	Omentectomy
Parametrectomy	Parametrectomy
Adhesiolysis	Adhesiolysis
General surgery	
Appendectomy	Appendectomy
Cholecystectomy	Cholecystectomy
Inguinal hernia repair	Inguinal hernia repair
	Ventral hernia repair
	Nissen fundoplication
	EndoStim implantation
	Decompression of celiac axis (treatment of Dunbar syndrome)
	Sleeve gastrectomy
Urological surgery	
	Adrenalectomy
	Prostatectomy
	Partial nephrectomy
	Renal cyst decortication
Thoracic surgery	
	Pulmonary lobectomy
	Pleural biopsy

TABLE 1.3 Fully reusable surgical instruments manufactured for the Senhance Surgical System.

3.0 mm
Atraumatic single-action grasper
Cobra grasper
DeBakey grasper
Needle holder
Monopolar Maryland dissector
Monopolar curved Metzenbaum scissors
5.0 mm
Allis grasper
Johan grasper
Kocher grasper
Strong grasper
Mixter dissector
Babcock forceps
Needle holder right
Needle holder left
Fundus grasper
Monopolar Maryland dissector
Monopolar curved Metzenbaum scissors
Monopolar L-Hook electrode
Bipolar large grasping forceps
Bipolar curved grasping forceps
Bipolar Maryland dissector insert
Bipolar curved scissors insert
Weck Hem-o-lock ML clip applier
10.0 mm
Right angle dissector
Weck Hem-o-lock ML clip applier

note is the addition of fully reusable 3-mm instruments, which augment and redefine MIS for robotic-assisted digital laparoscopy. In a report of one laparoscopic surgeon's experience with these smaller instruments and tips for hysterectomy ($n = 4$), the surgeon felt that the haptic feedback of the Senhance System allowed him to feel the flexibility of the instrument, which is especially important during careful minimally invasive traction and dissection [16]. The median operative time was 97.5 minutes (80−120 minutes) and estimated blood loss (EBL) was <50 mL. Patients were discharged on day 1 and no 30-day postoperative complications occurred.

1.3 User training and procedure planning

1.3.1 Training

The surgical team consists of the surgeon, the surgical assistant, and the surgical nurse, and training of the team is standardized in compliance with validated protocols approved in the EU by the CE and by the US FDA. The team is

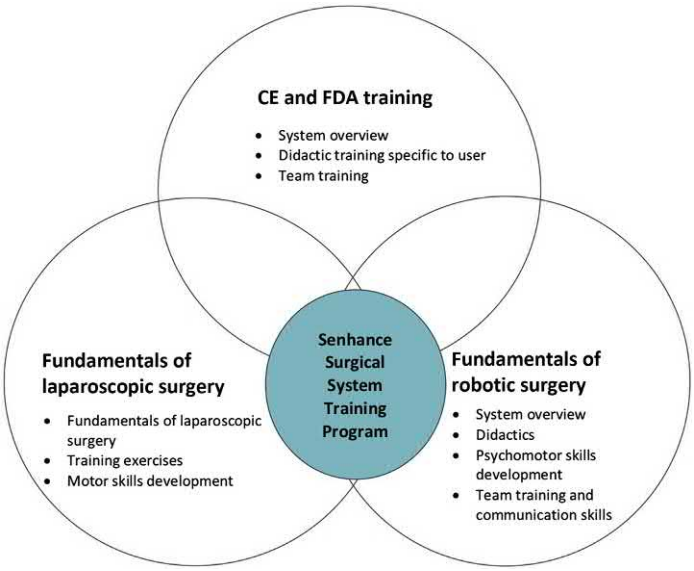

FIGURE 1.5 Senhance Surgical System training paradigm. *Credit: © 2018 TransEnterix, Inc.*

trained according to a general model (Fig. 1.5), which has been developed and was based upon recommendations of the Society of American Gastrointestinal and Endoscopic Surgeons to combine the fundamental elements of laparoscopic and robotic-assisted surgeries [17].

The purpose of the training is to facilitate surgeon, surgical assistant, and nurse training on the Senhance Surgical System and to provide trainers with all materials necessary to train a new user. All users of the Senhance Surgical System receive training specific to their roles. The objective is to provide users with the information and the opportunity to learn and practice skills required for safe and effective use and to enable interaction with the surgical system and its unique features before, during, and after a laparoscopic procedure.

Users receive 2 days of training defined by sequential modules, the last of which is a proficiency assessment based on mock case support. Users practice the skills they learned throughout the first day by performing a surgical procedure on the second day on a live porcine model. Each training session is attended by the three members of the surgical team. Users are advised to perform their first case within 1 week after training completion. Table 1.4 provides an outline of the training session; times are approximate, and breaks should be built into the days based on trainer and trainee discretion. A postmarket registry of all Senhance procedures and outcomes enables up-to-date evaluation of the system.

1.3.2 Procedure planning

The surgical team follows the same general procedural and operative room setup as for a traditional laparoscopic case. Specific considerations that are recommended are operating room table height, trocar positions, and manipulator arm placement. The operating room table height should not be so low or so high as to limit the motion of any of the manipulator arms during the course of the procedure. A visual guide—the "sweet spot"—is located on both the horizontal and vertical joints of each manipulator arm, and surgical teams are encouraged to recognize this guide and avoid placement of a manipulator arm too close to the end of its physical range of motion. Trocar positions should not be so close, that is, should not be less than 8 cm apart, so as to increase the possibility of arm collisions during surgery. In nearly all cases and patient populations, standard traditional port placement has been used without increased collision risk requiring special modification of the port placement. Consideration of the manipulator arm placement is according to preprocedure planning of the primary location of the surgical assistant to provide the assistant adequate room to access the perioperative space. The surgical team can consult recommended, procedure-specific manipulator arm placement diagrams to ensure adequate spacing for the intended location of the surgical assistant in the sterile field.

TABLE 1.4 Training session overview for the Senhance Surgical System.

Module	Method	Trainee role(s)	Time (h)	Learning objectives
Prior to arrival at the training facility				
Prelearning	Presentation with narrated videos	Surgeon, surgical assistant, nurse	1.5	Gain initial familiarity with the system. Receive system overview, including indications for use, features, and functionality.
Day 1				
Goals and expectations	Presentation (PowerPoint)	Surgeon, surgical assistant, nurse	0.5	Review the learning objectives for the subsequent modules.
Dry lab practicum	System hands-on/FLS tasks using trainer checklists	Surgeon, surgical assistant	2	Learn and practice the system skills required for effective use of the Senhance Surgical System. Focus on system setup, manipulator arm calibration and positioning, draping, instrument assembly, and instrument exchange.
	System hands-on using trainer checklists	Surgical assistant, nurse		Learn and practice the system skills required for effective use of the Senhance Surgical System. Focus on endoscope and instrument insertion, instrument exchange, cockpit orientation, and FLS tasks.
	Advanced Instrument (s) hands-on using trainer checklists	Surgeon, surgical assistant, nurse	2–5	Learn and practice the system skills required for effective use of the Senhance Surgical System Advanced Instrument(s). Focus on case preparation with sterile and nonsterile components, instrument exchange, cockpit orientation, and FLS tasks.
	Team training	Surgeon, surgical assistant, nurse	1	Practice team use of the system, including specific troubleshooting and communication among team members.
Day 2				
Pre-wet lab overview	Presentation (PowerPoint)	Surgeon, surgical assistant, nurse	1	Review differences between porcine and human anatomy to prepare for wet lab tasks.
Task-based wet lab and proficiency assessment	Porcine lab	Surgeon, surgical assistant, nurse	6	Practice the system skills required for effective use of the Senhance Surgical System and demonstrate proficiency by correctly completing tasks (no use errors) without trainer assistance. Nurse sets up the system and circulates according to role checklist. Surgical assistant supports patient-side tasks according to role checklist. Surgeon operates system according to role checklist.

FLS, Fundamentals of laparoscopic surgery.

1.4 Clinical findings

1.4.1 Gynecologic procedures

Many of the published clinical studies of robotic-assisted digital laparoscopy describe gynecologic procedures for the treatment of benign and malignant disorders.

1.4.1.1 Monolateral ovarian cyst removal

Gueli Aletti et al.'s first experience with Senhance was for a small homogeneous adult population of women ($n = 10$; BMI < 30 kg/m^2), who required monolateral ovarian cyst enucleation [9]. One experienced laparoscopic surgeon performed the procedures. There were no conversions to standard laparoscopy or to laparotomy and no intraoperative

complications. Median docking time was 6 minutes (range, 3−8 minutes), median operative time was 46.3 minutes (range, 22−80 minutes), and median EBL was 50 mL (range, 0−200 mL).

1.4.1.2 Heterogeneous series of gynecologic procedures

In a phase II single-center study of the safety and feasibility of Senhance in the hands of experienced laparoscopic surgeons for a heterogeneous series ($n = 146$) of gynecologic procedures (Group A: mono- or bilateral salpingo-oophorectomy or cyst enucleation, $n = 62$; Group B: myomectomy, $n = 4$; Group C: total hysterectomy, $n = 46$; and Group D: staging of endometrial cancer, $n = 34$), median docking time was 7 minutes (range, 3−36 minutes) [13]. Patients ranged in age from 19 to 79 years and the median BMI was 17.3 kg/m^2 (range, 17.3−34.0 kg/m^2). Over the course of the study, operative time lessened significantly for hysterectomy ($P < .001$) and adnexal procedures ($P < .002$). In both Group A and Group C, there were two conversions to standard laparoscopy. In Group D, one patient underwent laparoscopic conversion and two patients had conversion to laparotomy. This study was the first reported series of the novel robotic-assisted digital laparoscopic approach for the treatment of various gynecologic disorders. The procedures were successfully completed in 95.2% of the cases, with two reported complications (Group C: intraoperative, $n = 1$; postoperative, $n = 1$) for an overall complication rate of 1.4%. Intraoperative and early postoperative complication rates were similar to those reported for other minimally invasive gynecologic surgeries [18].

1.4.1.3 Senhance and standard laparoscopy for benign and malignant disease

A more recent, single-institution, case−control study provided a retrospective comparison of the safety and feasibility of Senhance and standard laparoscopy (control group) for total hysterectomy in women with benign (Fig. 1.6) and early malignant gynecologic disease (Fig. 1.7) [13]. A total of 203 women were enrolled (Senhance, $n = 88$; standard laparoscopy, $n = 115$). The median operative time was longer for the women in the Senhance group compared with that for women in the standard laparoscopy group (147 minutes; range, 58−320 and 80 minutes; range, 22−300, respectively). Noteworthy, however, was the comparability of the Senhance operative time to time reported for other robotic-assisted laparoscopic hysterectomy procedures. The longer operative times may have been attributable to learning a new surgical approach [19,20].

1.4.1.4 Hysterectomy in obese patients

Outcomes from a pilot study of the safety and feasibility of robotic-assisted digital laparoscopy for elective total extrafascial hysterectomy with bilateral salpingo-oophorectomy in obese (BMI ≥ 30 and < 40 kg/m^2) patients was recently reported [11]. Ten patients were enrolled (median BMI: 33.3 kg/m^2; range, 30.4−38.3 kg/m^2); the indication for each patient's procedure was early-stage (FIGO IA) endometrial cancer. Median docking time was 10.5 minutes (range, 5−25 minutes); median operative time was 110 minutes (range, 70−200 minutes); and median EBL was 100 mL (50−200 mL). No conversions to either standard laparoscopy or laparotomy occurred. The surgeons were experienced in laparoscopic techniques. They felt that the tactile feedback was especially important in terms of safety in this potentially challenging patient population.

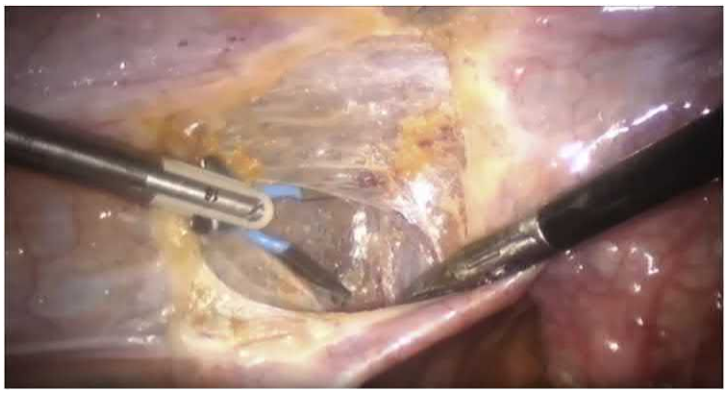

FIGURE 1.6 Mobilization of the uterine artery with advanced dissection during total hysterectomy using Senhance. *Credit: © 2018 TransEnterix, Inc.*

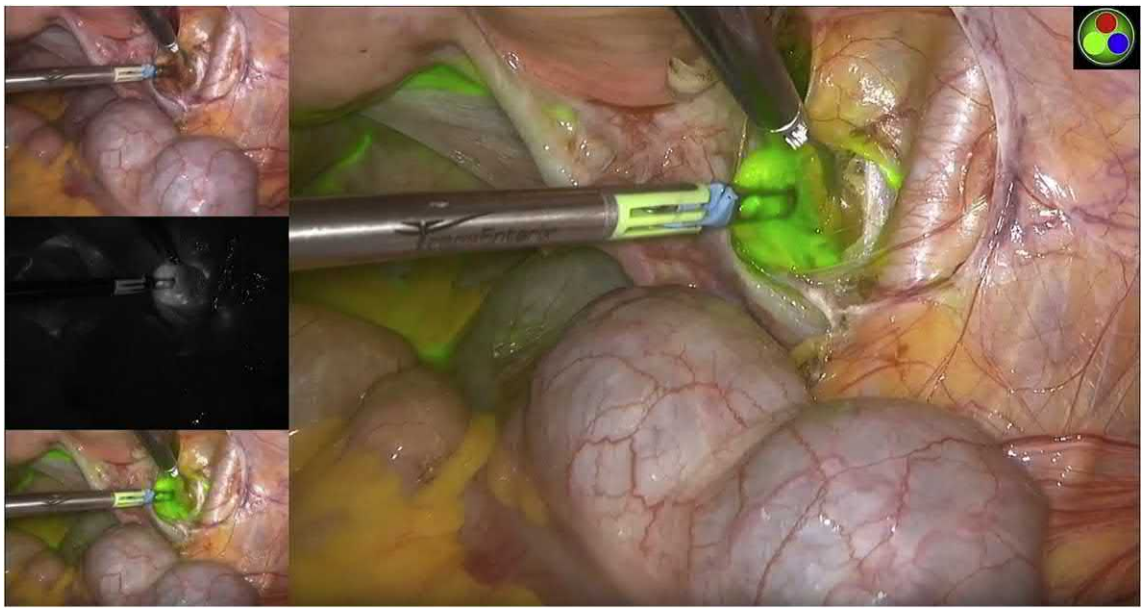

FIGURE 1.7 Robotic-assisted digital laparoscopic pelvic lymph node dissection aided by indocyanine green fluorescence imaging (Novadaq, Toronto, ON, Canada). *Credit: © 2018 TransEnterix, Inc.*

1.4.2 Colorectal disease

The first clinical experience with Senhance in the surgical treatment of patients ($n = 45$) with colorectal disease was recently reported by Spinelli et al. [15]. The heterogeneous surgical indications included: colorectal cancer (66%), complicated inflammatory bowel disease (18%), diverticular disease (11%), and endoscopically unresectable adenoma (4.4%). Median operating time for all of the procedures was 256 minutes and the median docking time was 10.7 minutes. Conversions were limited to three procedures that required conversion to standard laparoscopy; no procedures were converted to laparotomy. Median EBL for the entire cohort was <50 mL. Patients with malignant disease received R0 resections with disease-free margins, and the average number of nodes removed was 24.8. No device-related perioperative complications were reported. The authors reported that the system's haptic feedback may have been instrumental in preventing intraoperative complications.

1.4.3 Inguinal hernia repair

Stephan et al. described in detail their first experiences with Senhance in a consecutive adult population ($n = 116$) requiring primarily inguinal or ventral hernia repair, with some patients requiring cholecystectomy and a few requiring sigmoid resection for diverticular disease [6]. After approximately 30 procedures, the console time of inguinal hernia repair via the TAPP technique was comparable to the incision-to-suture time of a standard laparoscopic TAPP approach.

1.5 Cost considerations

The cost of ownership of robotic systems (acquisition, maintenance, and instruments) has been cited as a drawback to robotic-assisted surgery [21]. However, Senhance may provide a cost-effective robotic surgery program in light of its fully reusable instruments that can be used with conventional 5-mm trocars.

In 2016, Rossitto et al. reported the first one-way sensitivity analysis of costs associated with the use of Senhance in a consecutive series of procedures for the treatment of early-stage endometrial cancer or benign uterine disease in low-risk patients [22]. The procedures, which were performed by three experienced laparoscopic surgeons, were hysterectomy and bilateral salpingectomy ($n = 13$), radical hysterectomy and bilateral salpingo-oophorectomy ($n = 50$), and radical hysterectomy bilateral salpingo-oophorectomy and pelvic lymphadenectomy ($n = 18$). The average cost per patient for all of the procedures was €3391.82 and consisted of an average surgical staff cost of €1493.06, operating

room cost of €1225.66, and equipment cost of €673.09. Equipment, which did not include depreciation costs, represented 19.8% of the average procedure cost.

Rossitto's paper provides an improved understanding of healthcare resource allocation with the Senhance Surgical System in commonly performed gynecologic surgeries: the costs and outcomes of a robotics program based on Senhance may be similar to many programs involving traditional laparoscopic procedures. Future economic studies might include case-controlled and comparative analyses describing direct and indirect costs associated with perioperative outcomes for hernia repair, colorectal procedures, upper gastrointestinal procedures, prostatectomy, and thoracoscopic surgeries.

1.6 Conclusion

Published clinical data support the clinical safety, efficacy, and economic feasibility of digital laparoscopy with the Senhance Surgical System in the treatment of a variety of benign and malignant disorders. The system provides novel robotic-assisted benefits to the surgical team with rapid docking and a short learning curve as well as cost of ownership that is comparable to standard laparoscopy.

Acknowledgment

The authors thank Conor Carlsen (TransEnterix, Inc.) for facilitating the development of this chapter.

References

[1] Park A, Lee G, Seagull FJ, Meeneghan N, Dexter D. Patients benefit while surgeons suffer: an impending epidemic. J Am Coll Surg 2010;210(3):306–13.

[2] Miller K, Benden M, Pickens A, Shipp E, Zheng Q. Ergonomics principles associated with laparoscopic surgeon injury/illness. Hum Factors 2012;54(6):1087–92.

[3] Dimou FM, Eckelbarger BS, Riall TS. Surgeon burnout: a systematic review. J Am Coll Surg 2016;222(6):1230–9.

[4] Grisham S. Medscape general surgeon lifestyle report 2018: personal happiness vs work burnout, <https://www.medscape.com/slideshow/2018-lifestyle-surgeon-6009226#4>; 2018 [accessed 23.06.18].

[5] Hutchins AR, Manson RJ, Lerebours R, Farjat AE, Cox ML, Mann BP, et al. Objective assessment of the early stages of the learning curve for the Senhance surgical robotic system. J Surg Educ 2018;76:201–14. Available from: https://doi.org/10.1016/j.jsurg.2018.06.026 [Epub ahead of print].

[6] Stephan D, Sälzer H, Willeke F. First experiences with the new Senhance telerobotic system in visceral surgery. Visc Med 2018;34:31–6. Available from: https://doi.org/10.1159/000486111.

[7] Stark M, Pomati S, D'Ambrosio A, Giraudi F, Gidaro S. A new telesurgical platform—preliminary clinical results. Minim Invasive Ther Allied Technol 2015;24(1):31–6. Available from: https://doi.org/10.3109/13645706.2014.1003945.

[8] Gueli Alletti S, Rossitto C, Cianci S, Restaino S, Costantini B, Fanfani F, et al. Telelap ALF-X vs standard laparoscopy for the treatment of early-stage endometrial cancer: a single-institution retrospective cohort study. J Minim Invasive Gynecol 2016;23(3):378–83. Available from: https://doi.org/10.1016/j.jmig.2015.11.006.

[9] Gueli Alletti S, Rossitto C, Fanfani F, Fagotti A, Costantini B, Gidaro S, et al. Telap Alf-S–assisted laparoscopy for ovarian cyst enucleation: report of the first 10 cases. J Minim Invasive Gynecol 2015;22(6):1079–83.

[10] Gueli Alletti S, Rossitto C, Cianci S, Scambia G. Telelap ALF-X total hysterectomy for early stage endometrial cancer: new frontier of robotic gynecological surgery. Gynecol Oncol 2016;140(3):575–6. Available from: https://doi.org/10.1016/j.ygyno.2016.01.018.

[11] Gueli Alletti S, Rossitto C, Cianci S, Perrone E, Pizzacalla S, Monterossi G, et al. The Senhance surgical robotic system ("Senhance") for total hysterectomy in obese patients: a pilot study. J Robotic Surg 2018;12(2):229–34. Available from: https://doi.org/10.1007/s11701-017-0718-9.

[12] Fanfani F, Restaino S, Gueli Alletti S, Fagotti A, Monterossi G, Rossitto C, et al. TELELAP ALF-X robotic-assisted laparoscopic hysterectomy: feasibility and perioperative outcomes. J Minim Invasive Gynecol 2015;22(6):1011–17. Available from: https://doi.org/10.1016/j.jmig.2015.05.004.

[13] Fanfani F, Monterossi G, Fagotti A, Rossitto C, Gueli Alletti S, Costantini B, et al. The new robotic TELELAP ALF-X in gynecological surgery: single-center experience. Surg Endosc 2016;30(1):215–21. Available from: https://doi.org/10.1007/s00464-015-4187-9.

[14] Fanfani F, Restaino S, Rossitto C, Gueli Alletti S, Costantini B, Monterossi G, et al. Total laparoscopic (S-LPS) versus TELELAP ALF-X robotic-assisted hysterectomy: a case-control study. J Minim Invasive Gynecol 2016;23(6):933–8. Available from: https://doi.org/10.1016/j.jmig.2016.05.008.

[15] Spinelli A, David G, Gidaro S, Carvello M, Sacchi M, Montorsi M, et al. First experience in colorectal surgery with a new robotic platform with haptic feedback. Colorectal Dis 2017. Available from: https://doi.org/10.1111/codi.13882 [Epub ahead of print].

[16] Gueli Alletti S, Perrone E, Cianci S, Rossitto C, Monterossi G, Bernardini F, et al. 3 mm Senhance robotic hysterectomy: a step towards future perspectives. J Robotic Surg 2018;12(3):575–7. Available from: https://doi.org/10.1007/s11701-018-0778-5.

[17] Brunt M. Bulletin No. 11 Fundamentals of laparoscopic surgery: celebrating a decade of innovation in surgical education. American College of Surgeons; 2014. p. 99.
[18] Fanfani F, Fagotti A, Rossitto C, Gagliardi ML, Ercoli A, Gallotta V, et al. Laparoscopic, minilaparoscopic and single-port hysterectomy: perioperative outcomes. Surg Endosc 2012;26:3592–6.
[19] Rosero EB, Kho KA, Joshi GP, Giesecke M, Schaffer JL. Comparison of robotic and laparoscopic hysterectomy for benign gynecologic disease. Obstet Gynecol 2013;122:778–86.
[20] Rossitto C, Gueli Alletti S, Fanfani F, Fagotti A, Costantini B, Gallotta V, et al. Learning a new robotic surgical device: Telelap Alf X in gynaecological surgery. Int J Med Robotics Comput Assist Surg 2016;12(3):490–5.
[21] Lotan Y. Is robotic surgery cost-effective: no. Curr Opin Urol 2012;22:66–9.
[22] Rossitto C, Gueli Alletti S, Romano F, Fiore A, Coretti S, Oradei M, et al. Use of robot-specific resources and operating room times: the case of Telelap Alf-X robotic hysterectomy. Int J Med Robotics Comput Assist Surg 2016;12:613–19. Available from: https://doi.org/10.1002/rcs.1724.

2

A Technical Overview of the CyberKnife System

Warren Kilby, Michael Naylor, John R. Dooley, Calvin R. Maurer, Jr. and Sohail Sayeh

Accuray, Sunnyvale, CA, United States

CHAPTER FOCUS
ENGINEERING

TECHNOLOGY
ROBOTIC & IMAGE-GUIDED

LINK TO
VIDEO

ABSTRACT

The CyberKnife System is a frameless, image-guided robotic technology used to deliver stereotactic radiosurgery and radiotherapy anywhere in the body where it is clinically indicated. The treatment procedure is automated and delivered under user supervision. Throughout treatment the radiosurgical target is continually sensed using a combination of X-ray and optical imaging. The target pose is localized into a common reference frame using a combination of image registration algorithms and precisely calibrated coordinate transformations. A robotic couch, on which the patient is positioned, and a robotic treatment manipulator on which a medical linear accelerator is mounted, are aligned using this localization. Manipulation is achieved by delivering ionizing radiation to the target using a high-energy X-ray beam generated by the linear accelerator. Treatment involves delivery of a large number of nonoverlapping treatment beams, from a noncoplanar workspace, that allows sufficient radiation dose to be delivered to the target while respecting the dose tolerances of surrounding healthy tissues. The radiation dose delivered by each beam is determined by a 2D modulated fluence pattern controlled by variable beam collimation, linac dose control, and robot pointing. Pretreatment planning involves segmenting the target and healthy organ volumes using multimodality medical imaging, and using this to optimize the set of beam directions and the modulated fluence pattern for each beam. This chapter describes the CyberKnife System technology, and its major subsystems, as current in 2019.

Handbook of Robotic and Image-Guided Surgery. DOI: https://doi.org/10.1016/B978-0-12-814245-5.00002-5

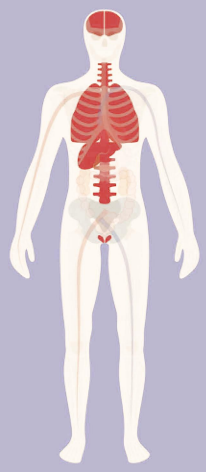

LUNG BRAIN BREAST SPINE PROSTATE LIVER

2.1 Introduction

Stereotactic radiosurgery (SRS) is a noninvasive alternative to conventional surgery using precisely targeted beams of ionizing radiation directed from outside the patient to replace the surgical resection of solid tumors, other lesions, or functional targets. SRS was originally developed for intracranial applications and required the use of a stereotactic frame mechanically attached to the patient's skull to achieve the required beam alignment precision. Treatment was delivered in a single session (or treatment fraction) using multiple beams distributed over a large solid angle [1]. Subsequently, the same general principles have been applied with new technologies to treat extracranial targets, either as an alternative to, or in combination with, conventional surgery and radiation therapy. Such extracranial treatment is commonly referred to as stereotactic body radiation therapy (SBRT) [2] or stereotactic ablative radiotherapy (SABR) [3], the subtle distinctions between which are beyond the scope of this chapter. Current SRS/SBRT/SABR (hereafter referred to collectively as *radiosurgery*) techniques use either mechanical frame-based or imaging-based stereotactic alignment, and are typically delivered in one to five treatment fractions. Common clinical indications include intracranial targets [malignant and benign tumors, arteriovenous malformations (AVMs), and functional diseases], spinal tumors and AVMs, and malignancies in the lung, prostate, liver, head and neck, and other sites, including both primary and metastatic diseases [4,5].

A fundamental difference between radiosurgery and conventional radiation therapy is that the former employs more aggressive dose-fractionation schemes. Since all radiation treatment is limited by toxicity to healthy tissues, this requires that radiosurgery achieves higher levels of geometric accuracy and dose conformality than conventional radiation therapy, as outlined as follows.

1. Geometric accuracy: The geometric uncertainties associated with aligning external treatment beams to a clinical target volume (CTV) within the body are usually managed by adding margins to the CTV during the treatment planning phase to form a planning target volume (PTV) [6]. Delivering the prescription dose to the entire PTV ensures that the CTV receives the intended dose. The CTV−PTV margin is a combination of setup and internal margins [7]. The setup margin includes the uncertainties in localizing the CTV at the start of each treatment in the same frame of reference as the treatment device, and of aligning the treatment beams to the CTV in this frame. The internal margin accounts for intratreatment motion of the CTV after initial localization. The most common example is respiratory motion, which affects targets within the lung, liver, pancreas, and kidneys. However, clinically relevant internal motion also affects the gastrointestinal and genitourinary systems (e.g., changes in bladder filling or rectal content during treatment can significantly alter the pose of a prostate cancer CTV [8,9]), and for essentially all target locations when gross patient movements are considered. The latter are usually limited by patient immobilization devices, but movements of a few millimeters are observed over typical treatment periods even for immobilized patients with intracranial or spinal CTVs [10]. Accommodating geometric uncertainties using margins is problematic when the CTV is adjacent to radiosensitive healthy tissues (e.g., lung, liver, or brain tissue surrounding a tumor, or the bladder and rectum adjacent to a prostate cancer CTV) since parts of these healthy tissues overlap the PTV and receive the full prescribed dose. These overlaps limit the dose-fractionation that can be employed, especially when complications are associated with relatively small volumes of healthy tissue receiving high doses.
2. Dose conformality: The physical nature of radiation transport means that dose deposition cannot be limited to the PTV only, but also spills out into the surrounding healthy tissues. In the standard nomenclature, the volume of tissue receiving the prescription dose is the treated volume (TV), and the volume receiving a dose that is significant in terms of normal tissue tolerance is the irradiated volume (IV) [6]. A perfect treatment would limit the TV to be identical to the PTV and have an infinite dose gradient in all directions beyond the TV such that the TV to IV expansion is zero. Neither of these is practically achievable. The PTV to TV expansion is generally determined by the way in which the incident radiation fluence from each treatment beam is modulated (e.g., by collimating the beam to the precise projection of the CTV using a collimation system that achieves very narrow beam penumbra and very low transmitted fluence outside of the collimated area). The TV to IV expansion is determined by the radiation modality and by the number of treatment beams used and their spatial arrangement. Dose gradients are maximized when many nonoverlapping beams are used. This makes use of noncoplanar beam arrangements distributed across a large solid angle beneficial.

The CyberKnife System provides a method for frameless radiosurgery, enabling treatment to be delivered anywhere in the body where it is clinically indicated. Radiosurgery delivered by CyberKnife is autonomous but delivered under human operator supervision. The treatment paradigm involves a combination of image-based alignment, robotic manipulation of the treatment beam and patient, continual image-based tracking of the target throughout treatment, and use of

a large noncoplanar workspace. This paradigm can be employed anywhere in the body and is used for every treatment delivered by the system. CyberKnife was conceived in 1992 [11] and first fully described in 1997 [12]. The system received FDA approval for intracranial treatment in 1999, which was extended to include extracranial treatment in 2001. To date, it is estimated that over 400,000 patients have been treated worldwide using CyberKnife, covering the full range of clinical indications described above. In the 25 years since its inception the technology has undergone continual development such that almost no component remains unchanged from the original design. A complete technical description of the system was published most recently in 2010 [13]. There have since been major changes to several key subsystems and the introduction of a major new system version. This chapter will therefore provide the first technical overview of the CyberKnife M6 System, as current in 2018.

2.2 System overview

The treatment room shown in Fig. 2.1 illustrates the layout of the major treatment delivery subsystems. The patient lies on a flat couch top and except in some pediatric procedures is fully conscious throughout treatment. The couch is supported by a 6 degrees of freedom (6DOF) robotic manipulator that enables the patient pose to be adjusted along all six translational and rotational axes. At the head of the treatment couch is another 6DOF robotic manipulator supporting a medical linear accelerator (linac) that generates the treatment beam. This treatment manipulator allows beams to be directed without the isocentric pointing or coplanar workspace constraints of a traditional C-arm linac gantry. Next to the treatment manipulator is a pedestal in which exchangeable secondary collimator assemblies are stored when not in use. Above the couch are two ceiling-mounted X-ray tubes. These produce square imaging beams directed toward the floor, the central axes of which are each at 45 degrees to the vertical. Image detection is accomplished using two flat panel X-ray detectors mounted flush to the floor. The point in space where the central axes of the two imaging beams intersect is the *machine center*. The treatment manipulator is positioned such that beams can be directed from many noncoplanar directions toward points within a treatment volume, which is a region of space surrounding the machine center. Treatment accuracy relies on the position and orientation of the imaging system with respect to the treatment manipulator being known with high precision, which is ensured by mechanical alignment during installation and calibration procedures performed during system commissioning.

To supplement the X-ray imaging system, an optical imaging system is used for treatments in which respiratory motion is tracked in real time. An array of three optical cameras is installed in a ceiling-mounted boom-arm which can be swung out of the way when not in use. During respiratory motion tracking, the camera is used to continuously measure the position of three optical markers attached to a vest worn by the patient. These major subsystems are described in more detail in Section 2.3.

Because of the radiation hazard of the treatment beam, the system is installed within a shielded bunker. During treatment delivery, the operators (usually radiation therapists) monitor the system from a control room situated outside the treatment room. This control area, as shown in Fig. 2.1, contains the treatment delivery computer. This displays the live X-ray images acquired during treatment and pregenerated digitally reconstructed radiographs (DRRs), target location tracking results, and information about each treatment beam including the dose delivered and beam collimation settings. Once commenced, treatment proceeds autonomously unless errors are detected or the operator pauses delivery. Because the radiation shielding makes it impossible for the operators to view the patient directly the treatment room is fitted with CCTV, and an intercom enables the patient and operators to communicate during treatment. Additional system hardware, including controllers for the two robotic manipulators, linac, and imaging systems, power distribution equipment, linac cooling and gas systems, and a patient database computer, is installed in a separate equipment room close to the treatment room.

The first step in the treatment process is treatment planning, as illustrated in Fig. 2.2. Vendor-provided treatment planning software (TPS) is installed on one or more computers, usually situated in a separate planning office. Each TPS allows a simulation of the treatment delivery in which the optimum geometric arrangement of treatment beams and radiation fluence per beam is determined. The planning process starts with acquisition of a three-dimensional (3D) CT, which is transferred to the TPS via a dedicated patient database. A 3D patient model is built from the planning CT, in which a patient coordinate system is defined and the tissue density at each voxel is calculated. Target volumes and relevant healthy tissues are segmented within this model using a combination of automatic and manual methods. To aid tissue segmentation, multimodality secondary image sets can be registered to the primary CT scan. A virtual alignment of the treatment imaging system to the patient model is then performed, such that the treatment target is close to the virtual machine center. This defines the transformation from the patient coordinate system to the virtual imaging system, and since the imaging system to treatment manipulator transformation is already known, this enables a set of

FIGURE 2.1 The CyberKnife treatment suite. The left image shows the patient lying on a flat couch mounted on a robotic manipulator, with the linear accelerator mounted on a second robotic manipulator at the head of the couch. In this case the multileaf collimator assembly is shown attached to the treatment robot. Behind the patient and treatment robot in this image is the pedestal used to store the three alternative secondary collimator assemblies when not attached to the treatment robot. The two ceiling-mounted X-ray tubes are shown, with the floor-mounted X-ray image detectors housed under the rectangular green panel beneath the couch. The optical camera array in its ceiling-mounted boom-arm is shown near the left side of the image. The right image shows the control area. The treatment delivery computer to the left displays live X-ray images, DRRs, tracking results, and treatment-related data during treatment. To the right, the CCTV and intercom systems monitor and communicate with the patient during treatment. The small white console next to the keyboard contains low-level controls to initiate and interrupt treatment. *DRR*, Digitally reconstructed radiograph. *Control area image courtesy Dr. J.A. Gersh, Gibbs Cancer Center and Research Institute—Pelham, Greer, SC, United States.*

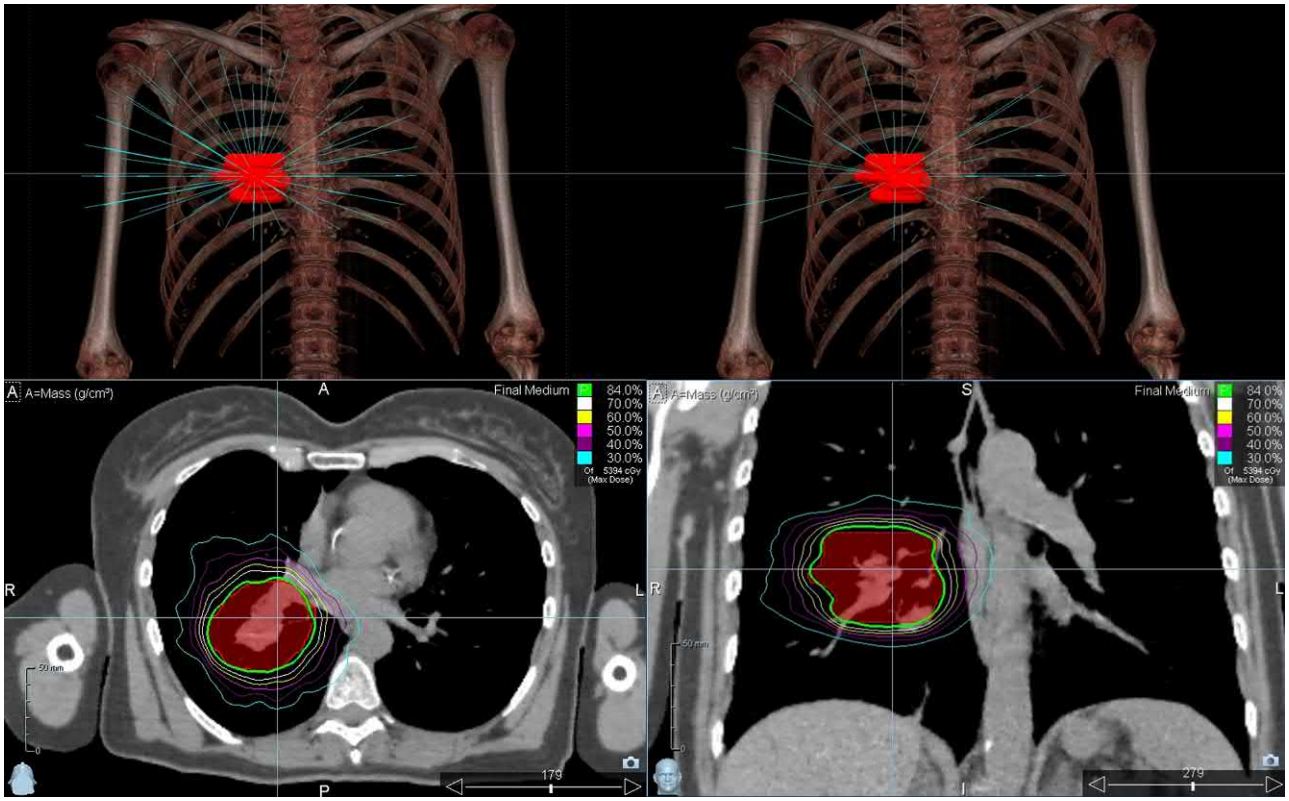

FIGURE 2.2 An example treatment plan for a lesion in the right lung. Top-left shows an anterior view of the 3D patient model (for simplicity the tissue density has been windowed to show only bone, and the only segmented structure is the PTV, shown in red). The *blue lines* show 100 noncoplanar beam directions that are available to treat this target. Each line corresponds to a position and orientation of the treatment robot relative to the patient that does not violate robot joint, cable management, or collision constraints. Top-right shows the subset of 24 beams which in this case were selected during the treatment plan optimization. The bottom panels show axial and coronal sections of the CT scan. The dose distribution resulting from the optimized set of beam directions and beam fluence is shown by the *colored isodose lines* (connecting points of constant dose). In this case the conformality of the treated volume (within the green line) to the PTV is high, as is the dose fall-off in all directions (shown by the closely spaced *isodose lines* outside the PTV). These are among the dose representations that the treating physician will typically review before approving the plan for treatment. *3D*, Three-dimensional; *PTV*, planning target volume.

virtual treatment beams to be defined onto the patient model corresponding to achievable treatment manipulator orientations. Typically, more than 100 of these feasible beam orientations are found. Using this simulation, the operator selects the optimal set of beam directions and radiation fluence per beam. This complex task is usually performed with the aid of automated optimization algorithms implemented within the TPS. The methods used for image registration, segmentation, dose calculation, and plan optimization are described in more detail in Section 2.3. The resulting dose distribution is reviewed and approved by the treating clinician (usually a radiation oncologist or neurosurgeon) prior to treatment, and the approved plan is stored in the patient database. From the approved plan a set of machine instructions needed to deliver the treatment is automatically generated. In addition, a set of DRRs is generated by ray-casting through the 3D CT model using the simulated orientation of the X-ray imaging system relative to the patient.

Prior to treatment, the plan is transferred to the treatment delivery computer. Treatment alignment is based on registering live stereoscopic X-ray images to the precalculated DRRs generated from the treatment plan. Each 2D image registration is calculated automatically using skeletal anatomy (either skull or spinal vertebrae), lung tumor, or implanted fiducial markers (the details of these registration algorithms are provided in Section 2.3). The results of the 2D registrations are combined by geometric back projection to give a 3D transformation of the target anatomy in the live images to the corresponding anatomy in the planning 3D model. The registration result contains the change in the target pose (3D position and 3D rotation) within the treatment room with respect to the simulated geometry in the treatment plan. Initially the couch manipulator is adjusted to grossly align the patient, such that these offsets are relatively small (typically a few millimeters and degrees). Once this is accomplished the couch remains static during

treatment, and all fine alignment corrections are achieved by adjusting the treatment manipulator position and orientation from the settings stored in the treatment plan based on the target pose deviation and the known transformation from imaging system to treatment manipulator system. Using the treatment manipulator rather than the couch manipulator to perform the fine alignment is important, as it removes the need for the patient to be considered as a rigid object statically attached to the couch. Intratreatment motion is tracked continually by repeating the cycle of X-ray acquisition—image registration—pose deviation calculation—treatment manipulator correction throughout treatment, typically every 30−60 seconds. The exception to this alignment strategy is for targets affected by respiratory motion, which move too rapidly to be managed at this imaging frequency. In these cases, the optical camera system is used to monitor the position of markers positioned on the patient surface in real time (approximately every 10 ms). Prior to treatment the correlation of external marker positions to internal target positions is calculated using a series of X-ray images acquired at multiple phases of the breathing cycle. During treatment the real-time optical signal is combined with this correlation model to sense the target position in real time, which is used to determine the treatment manipulator corrections needed to track the target in real time and maintain the same static beam-target orientation that was simulated in the treatment plan. Additional intratreatment X-ray images are used to verify and adapt the correlation model throughout treatment. More detail of this respiratory tracking technology is provided in Section 2.3.

The most meaningful definition of geometric accuracy with any radiosurgery system is the *total system error* (TSE) of the entire treatment planning and delivery sequence (a measurement originally developed for frame-based radiosurgery and termed "total clinically relevant error" [14]). With CyberKnife this is most commonly tested using a phantom containing a hidden spherical target object in which two radiochromic films are mounted orthogonally. The phantom is CT scanned using the standard patient protocol, a treatment plan is developed that encloses the target with a conformal spherical dose distribution, and this plan is then delivered to the phantom. The vendor specification for the radial offset between the dose centroid measured on the films and the intended position (center of the spherical target) is ≤ 0.95 mm. Versions of this phantom enable the test to be performed for all anatomical tracking methods (skull, spine, lung tumor, and fiducial marker tracking), and with real-time phantom motion to simulate respiratory motion. The TSE combines uncertainties in the full treatment process, including CT acquisition, image segmentation, dose calculation and plan optimization, X-ray to DRR registration, treatment beam alignment, and dose delivery. TSE is measured during acceptance testing and periodic quality assurance tests with every CyberKnife System to demonstrate that this accuracy specification is maintained. A summary of user-published TSE results is provided in tables II and IV of Kilby et al. [13].

2.3 Major subsystems

2.3.1 Robotic manipulation

2.3.1.1 Treatment manipulator

The treatment manipulator for the CyberKnife M6 System is the KUKA QUANTEC KR300 R2500 Ultra robot. This is a 6DOF robot with a maximum payload of 300 kg, 2496 mm reach, and position repeatability of ± 0.06 mm. A primary reason for selecting this robot was the higher payload required for the addition of the multileaf collimator (MLC) (described later)—the KR300 has a 60 kg maximum payload increase over the treatment manipulator used in the CyberKnife VSI system [13]. The increased payload comes with a trade-off in overall reach of the robotic arm—approximately a 200 mm reduction in maximum reach. This required changing the treatment room layout in two ways. First, the robot was moved from 45 degrees superior-lateral to the patient to be in-line superior to the patient. Second, a custom pedestal was designed to raise the robot 412 mm off the floor, allowing the system to reach over the patient and maximize the available workspace for delivery.

Cable management, predominantly to support the operation of the linac and other devices in the treatment head, as well as industrial design are added to the KUKA robot (Fig. 2.3). The conduit for the cable management is 95 mm in diameter and carries dozens of cables including sensors for beam collimation systems, power and signal cables for the monitor chamber and dosimetry electronics, a pneumatic air hose, and high-energy cabling for the linac. The cable management is designed to support the full range of robot motion throughout its workspace—this results in a 750 mm extendable range of the conduit when the robot is stretched out, but also requires that the cabling retracts when the robot head is superior to the patient. A tensioning mechanism is located at the elbow joint to ensure that the cabling is retracted as needed while maintaining minimum bend radii in all cases.

FIGURE 2.3 The treatment robot showing the KUKA robot, treatment head, cabling and tensioning mechanism, and pedestal (left), and in the treatment room with industrial covers fitted together with the treatment couch and Xchange table (right).

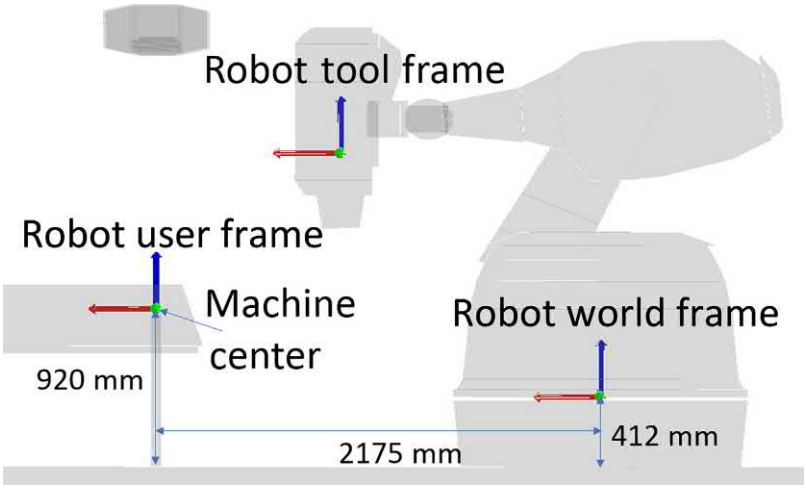

FIGURE 2.4 Lateral view of robot system coordinate frames. Red is + *X*, blue is + *Z*, and green is + *Y*.

2.3.1.2 *Coordinate systems and treatment workspace calibration*

There are three primary coordinate frames when describing the robot workspace within the treatment room (Fig. 2.4). The robot world frame has its origin at the base of the robot, centered on the first axis of rotation where the robot is mounted on top of the pedestal. The robot tool frame is defined by a laser mounted inside the linac, such that the laser is coincident with the radiation beam, and the origin is the treatment X-ray beam source (center of the linac target). The robot user frame is defined with its origin at the machine center, with rotations aligned to the robot world frame.

The treatment volume for the CyberKnife is centered at the machine center. This point is nominally 2175 mm + *X* and 508 mm + *Z* in the robot world frame—when combined with the pedestal, this gives a height of 920 mm off the floor. To calibrate the exact position of this point relative to the robot, a calibration post is inserted into a floor frame

which provides a reference point. The calibration of the robot relative to the machine center is performed using the linac laser to scan across a point like photodetector located at the tip of the calibration post. Scans of this point are performed from positions throughout the robot workspace and a least-squares minimization is found which provides the calibrated robot tool frame and origin of the user frame at the calibration point.

This provides a baseline calibration for the robot. However, to reach submillimeter accuracy throughout the entire clinical workspace, additional calibrations are required. Section 2.3.1.3 discusses the discretization of the workspace into "paths" and "nodes," as well as the next steps in system calibration.

2.3.1.3 Treatment paths and node properties

The available workspace that the robot can reach for clinical use is discretized into specific points, referred to as nodes, which are grouped into larger sets, referred to as paths. The robot can be oriented such that the treatment beam source (center of the linac X-ray target) is coincident with each node, and therefore nodes represent the source positions of treatment beams. Nodes are selected from a set of points located on concentric spheres about the machine center, with radii [referred to as source-to-axis distance (SAD)] ranging from 650 to 1200 mm. The node positions are selected to maximize robot reachability during real-time tracking of patient motion, as well as to provide flexibility for robot traversals to other nodes while avoiding collisions in the room and ensuring that the cable management is not stretched or compacted too much.

Separate paths are defined for different target anatomy and collimator types. The "head" path is designed such that the head portion of the couch top is located at the machine center. This is a smaller volume of the couch and leaves the section of the room between the couch top and the robot base open for treatment nodes. Fig. 2.5A shows the position of nodes in this path. This path has shorter SAD nodes (650−900 mm) to maximize the effective dose rate. The extracranial "body" path is designed for the couch extended fully superior to support placement of targets in the thorax or abdomen at the machine center. This path has longer SAD nodes (800−1200 mm) to allow for larger patient clearance due to respiratory motion tracking, prostate pitch tracking, and the larger range of possible alignment positions throughout the entire body (rather than just the center of the skull for the head path).

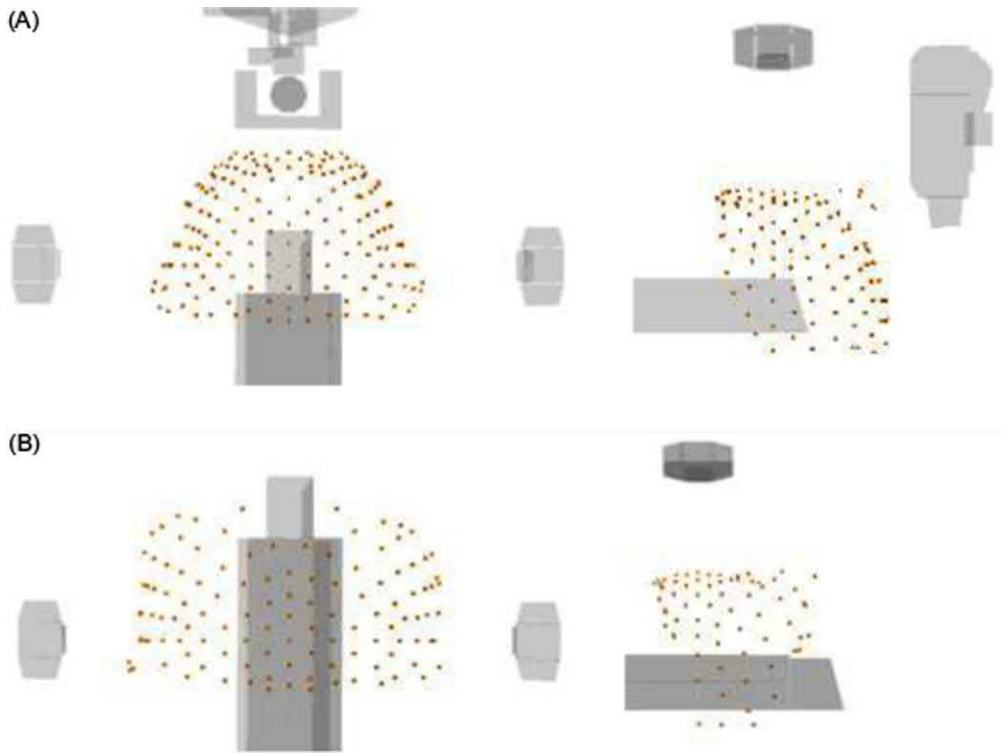

FIGURE 2.5 (A) Head path, seen from above (left) and from the side (right). Each *red dot* is a node. (B) Body path seen from above (left) and from the side (right). Each *red dot* is a node.

Although the fixed collimator housing and Iris collimator have the same external geometry, the MLC is very different, requiring different paths to handle this distinction (see Section 2.3.2 for a description of these secondary collimators). This results in four primary clinical paths, excluding those used for quality assurance. Each of these paths is calibrated independently, including separate calibrations for the fixed and Iris collimators due to mass differences. Path calibration consists of moving to each node in each path and performing a scan of the calibration post with the linac laser. This process generates a list of offsets which is applied at the delivery time. A final correction offset is measured using an arrangement of treatment X-ray beams directed at the machine center, to a phantom containing orthogonal X-ray-sensitive films (the TSE measurement described in Section 2.2). This combination of calibrations allows the system to achieve submillimeter accuracy in treatment beam delivery.

The path sets for the CyberKnife M6 System include 117 clinical nodes for the "body" Iris and fixed collimator path, 179 for the "head" Iris and fixed path, 102 for the "body" MLC path, and 171 for the "head" MLC path. These nodes, used as source points for delivering radiation, are referred to as "dose nodes." Each path also contains "dummy nodes" which are used only as traversal waypoints. Each node has associated data to inform the system how that node may be used from treatment planning through treatment delivery. This information includes maximum rotational and translational tracking corrections, X-ray imaging status (i.e., whether placing the treatment head at the node causes the treatment robot to obstruct one of the X-ray imaging systems), and a list of nodes in the path to which the robot can safely move, as well as an associated traversal time. The maximum tracking corrections guide the treatment planning system (TPS) to utilize the proper set of nodes given the parameters of the plan being created. For example, nodes used in prostate treatments require additional robot reachability to support ± 5 degrees of pitch correction, above the standard ± 1.5 degrees, while nodes used with real-time respiratory motion tracking must support ± 25 mm of translation corrections rather than the standard ± 10 mm. The X-ray imaging status of nodes is used to order the nodes appropriately so that there will be guaranteed imaging opportunities where the robot is not blocking either of the X-ray imaging devices. Once the dose nodes are selected during treatment planning, this provides the information required to do a traveling salesman optimization which minimizes the time spent moving between them. The traveling salesman algorithm is based on the Lin−Kernighan heuristic [15], but simplified and customized to work with the constraints and parameters for CyberKnife—primarily ensuring that imaging nodes are visited based on a custom time interval defined by the operator.

2.3.1.4 Collision avoidance and proximity detection

Although the paths were designed to avoid collisions with other components of the system, as well as a large bound on the patient volume, the system continuously monitors the position of each robot (treatment robot and patient couch) and calculates distances between these moving objects versus other moving components and static obstacles in the room. All objects are modeled as adjoining convex polytopes for the purposes of the proximity calculations. Fig. 2.6 shows an example of the polytopes when the robot is at a superior head path node, the colors are only to differentiate between separate models. It is important to note that the couch position can only act as a guide for the patient position, and depending on setup factors (pillows, blankets, pads, etc.), the patient may not be in the exact, expected position. The user can define one of a set of standard avoidance volumes around the couch based on the patient size and setup. The patient-facing portion of the collimator housing is also encased in a touch sensor so that if the patient reaches out to touch the robot, or there is a collision, an interlock is tripped that stops motion.

2.3.1.5 Xchange table and tool mounting calibration

One feature of the CyberKnife System is exchangeable secondary collimators via a pneumatic tool-changing mechanism. This enables rigid mounting of the linac and accurate calibration of the robot, while enabling the use of up to three different secondary collimation devices. To enable automated secondary collimator exchange, the storage table must be located and calibrated with respect to the robot. The tool-changing mechanics require submillimeter accuracy to operate, which requires a full 6DOF calibration of the table coordinate frame and sensor positions. The table has spots for three calibration posts, which are smaller versions of the one used for primary system calibration, and the calibration process moves the robot through a vertical and horizontal scan of each post. This provides three points, giving a full 6DOF representation of the table top plane relative to the robot. At the center of the storage well for each secondary collimator is another sensor. Each of these is scanned with the linac laser to calibrate the center of the well. In turn, the robot picks up and drops off each housing to ensure that the calibration scans successfully found the center positions. The bottoms of the wells are spring loaded, with overtravel sensors to monitor if the robot pushes down too far—while the tool mounting face of the linac has sensors to determine when a physical connection is made.

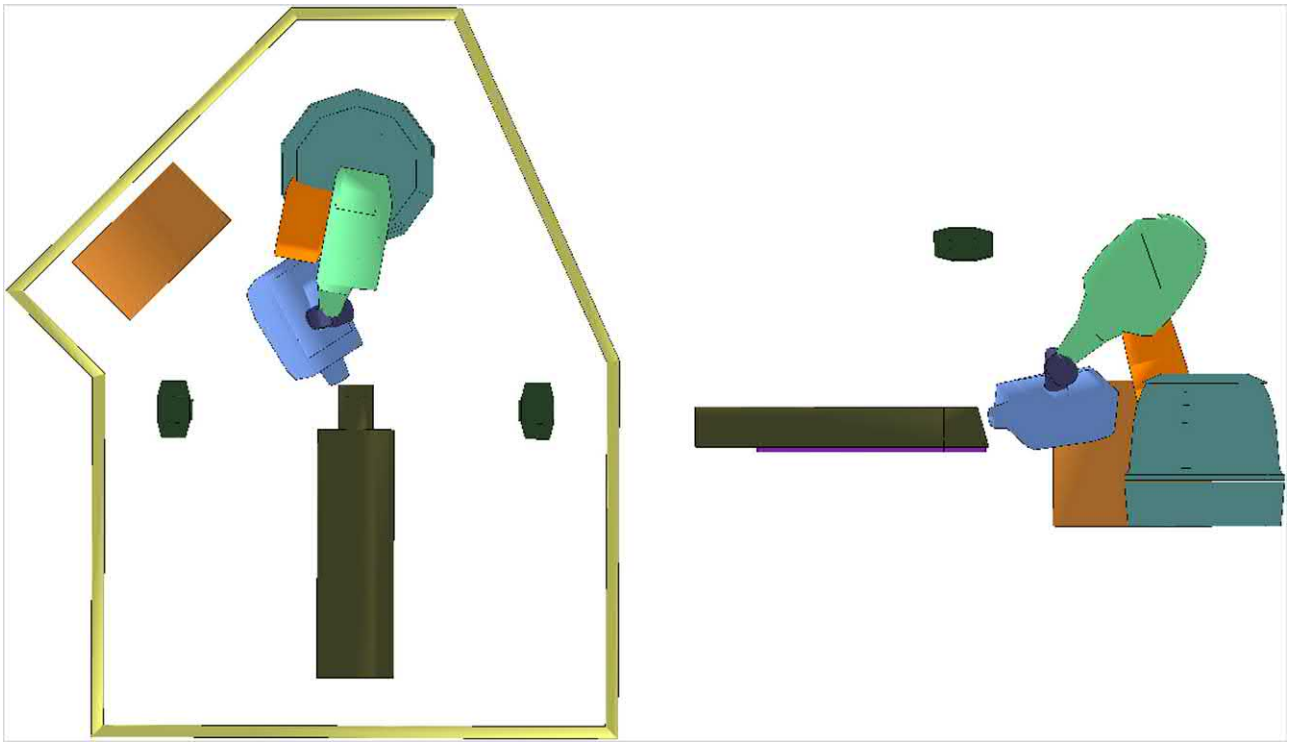

FIGURE 2.6 Example view of proximity detection modeling, with static and dynamic modeled components. The patient avoidance area around the couch is not shown.

The combination of the calibration procedure and these sensors allows the system to safely and quickly exchange between the different secondary collimators.

In addition to enabling the use of multiple collimator types, the table also enables the system to perform a laser alignment check prior to each treatment. This occurs either through a successful exchange of collimators or a single check of the laser value over the center of one of the housing wells. As the linac laser is aligned and calibrated with the treatment beam, this simple check ensures that the treatment beam is aligned consistently. This is checked prior to each treatment delivery.

2.3.1.6 RoboCouch

The patient couch (RoboCouch) is also a serial link manipulator which brings additional functionality to the CyberKnife System. RoboCouch is a custom-designed robot, based on the selective compliance articulated robotic arm (SCARA) configuration, which utilizes the same KUKA controller and KUKA wrist as the treatment robot. The first axis is a vertical axis to provide Z motion, with the two subsequent axes providing planar X/Y motion, followed by a three-axis intersecting wrist to enable rotation positioning (Fig. 2.7).

This design enables a therapist to fully align a patient in all 6DOF without having to physically adjust the patient inside the treatment room. The design of the couch provides the user with the ability to treat patients up to 500 lb, while maintaining submillimeter accuracy. The RoboCouch workspace allows for 100 cm of travel in the inferior/superior direction, while extending ± 18 cm in the patient left/right direction, and a minimum load height of ≤ 55 cm off the floor, which equates to 37 cm of travel posterior to the machine center. This workspace also includes nominal rotation ranges of ± 5 degrees about each axis, although there are reduced limits at the exterior of the translation limits. The combination of couch limits with the treatment robot tracking limits allows the CyberKnife flexibility with initial patient position on the couch, as well as to handle large patient movements without frequent manual adjustments of the patient.

The RoboCouch is calibrated to the rest of the CyberKnife System by performing a sequence of couch moves and tracking calibration targets using the X-ray imaging system. By correlating native couch coordinates to the imaging system coordinates, the system can accurately adjust the patient position based on imaging system results to maintain

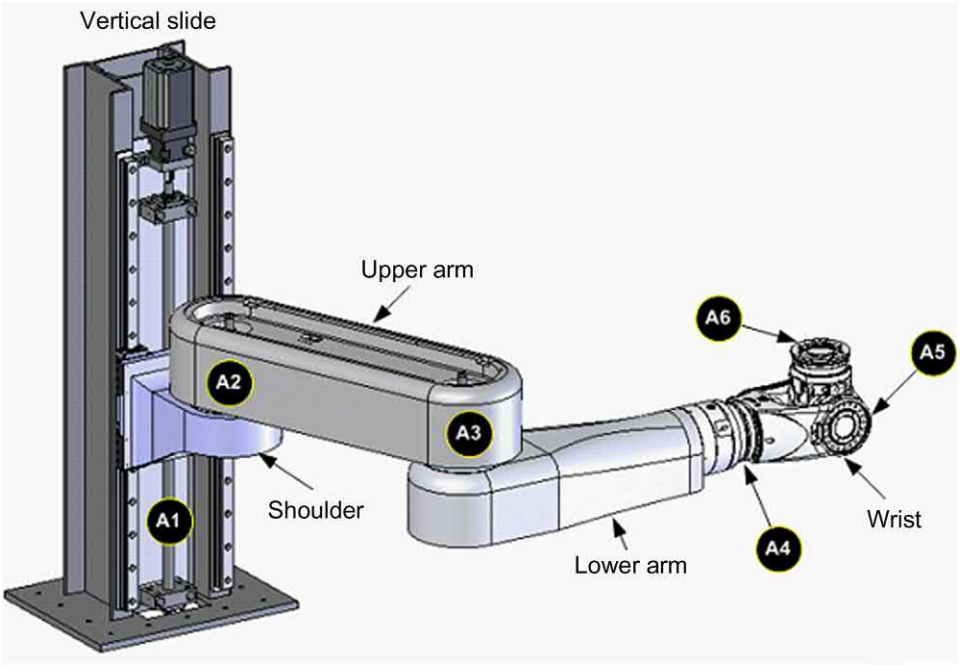

FIGURE 2.7 RoboCouch high-level diagram with axis labels.

patient alignment about the machine center. Once this calibration is performed, the CyberKnife utilizes the couch to adjust the patient position to nominal alignment with the DRRs, and then allows the treatment robot to adjust on-the-fly as the patient moves during treatment delivery.

2.3.2 Treatment head

The treatment head produces and controls the X-ray treatment beam. In the following description "up" is the direction along the beam central axis away from the patient, and "down" is toward the patient. The treatment head is mounted to the treatment manipulator and is divided into two parts (Fig. 2.8). The upper part is permanently attached, and the lower part is mechanically exchangeable for one of three alternatives. These lower head assemblies are stored in a pedestal next to the treatment robot base (Fig. 2.1) and are exchanged automatically by the treatment manipulator using a pneumatic tool-changing mechanism as described in Section 2.3.1.5.

The fixed (upper) part of the treatment head contains the linac which generates the treatment beam by accelerating electrons along an evacuated accelerator structure using microwave power, and colliding these accelerated particles with a thin metal target to generate X-rays principally through bremsstrahlung interaction. The linac is powered by an X-band cavity magnetron, also mounted in the treatment head, and delivers a 6 MV X-ray beam with a dose rate of 1000 cGy/min at the reference treatment distance of 800 mm from the beam source. The X-ray target is situated within the primary collimator, which is a large tungsten enclosure designed to minimize radiation leakage in all directions except along a fixed rectangular aperture defining the maximum possible treatment field size. Downstream of the target is the monitor chamber, which is a sealed, gas-filled ionization chamber used to control the dose delivered to the patient. Charge measured in this chamber is proportional to the X-ray fluence emitted by the linac. The relationship between this charge measurement and dose delivered to the patient is carefully characterized when the system is commissioned. During treatment, this signal is used to terminate each treatment beam when the radiation dose specified in the treatment instructions has been delivered. In addition, the chamber monitors the treatment dose rate, beam uniformity, and beam symmetry, and terminates treatment if these deviate outside a tolerable range. The laser–mirror assembly is aligned to direct the beam from a low-power optical laser mounted at right angles to the treatment beam along an axis coincident with the center of the radiation beam. The laser is not used therapeutically, but is essential for various quality assurance and calibration procedures and as part of the assembly exchange mechanism described previously.

The detachable part of the treatment head contains the secondary collimation system that defines the shape of the treatment beam incident on the patient. At the top of each of these is an intermediate collimator. This is fixed tungsten

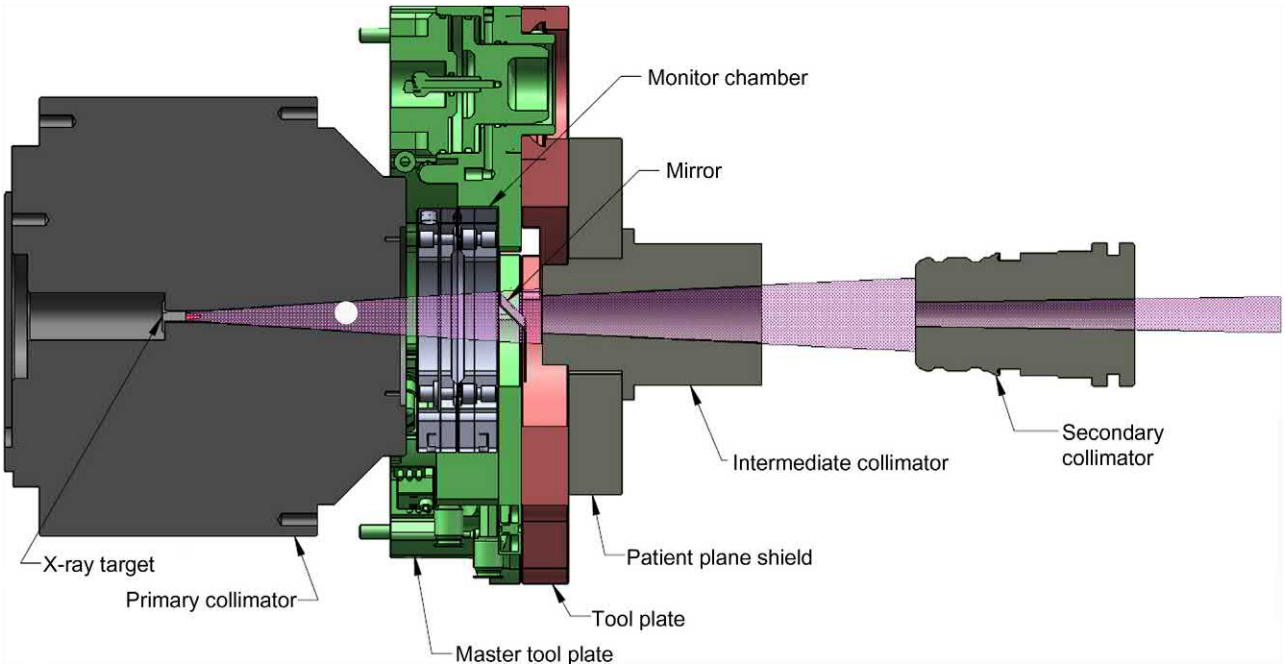

FIGURE 2.8 A section of the treatment head showing the major components responsible for shaping and controlling the treatment beam. The linear accelerator (not shown, to the left of this figure) directs a beam of electrons accelerated to approximately 6 MeV onto the X-ray target where they interact to generate the X-ray beam shown in purple. This beam is collimated by the combination of primary, intermediate, and secondary collimators to shape the beam that is incident on the patient (not shown, to the right of this figure). The electric charge created by the beam as it traverses the gas-filled monitor chamber is used to control the dose delivered to the patient. The 45 degrees mirror directs a low-power laser beam (not shown) that is coincident with the beam central axis. This is used for various quality assurance and other functions, but is not involved in treatment delivery. Automated pneumatic connection and disconnection of the master tool plate to tool plate allows alternate secondary collimator assemblies to be attached for each treatment. The fixed collimator assembly shown here is the simplest of these assemblies. The alternate secondary collimator assemblies (not shown) are an Iris variable circular aperture collimator, and a multileaf collimator.

shielding designed to reduce the field size from the maximum defined by the primary collimator down to the maximum supported by the variable secondary collimation sitting below, and to provide some additional shielding to the primary collimation. The three secondary collimator assemblies are described next.

1. Fixed conical collimators. These are 12 static tungsten cylinders, each with a circular aperture. The apertures define beam diameters (at 800 mm from the source) of 5−60 mm. The two smallest sizes have straight apertures. The others are focused to the beam source, which is important to achieve a sharp beam edge (i.e., to minimize the beam penumbra). The individual collimators are manually fitted within the fixed collimator assembly. The collimator size is sensed by the delivery system and an interlock prevents treatment delivery unless this matches the size contained in the treatment plan for each beam.
2. Iris variable aperture collimator. This collimator can replicate the same set of 12 circular field sizes as the fixed collimators without the need for any manual exchange of parts. It is formed by 12 triangular tungsten segments divided into two banks of six, mounted one above the other. Each bank defines a hexagonal beam aperture, and the two banks are rotated through 30 degrees with respect to each other to achieve a dodecagonal beam that closely approximates a circle. The rotational offset between the two banks also minimizes the radiation leakage between the segments, since any gap between segments in one bank is shielded by the body of a segment in the other. The upper bank forms a smaller aperture than the lower one to approximate the focusing of the fixed collimators. All 12 segments are driven using a single motor. This collimator assembly is described in greater detail elsewhere [16].
3. InCise MLC. This collimator can form irregular beam shapes within a maximum aperture of 115 mm × 100 mm (projected at 800 mm from the source). The beam collimation is provided by 52 tungsten leaves, divided into two opposing banks of 26, which move along linear trajectories orthogonal to the beam central axis. The leaves are driven independently and are capable of unlimited interdigitation and overtravel. The edges of the treatment beam are collimated either by the tips or sides of the leaves. To minimize beam penumbra, the leaf tips have a three-sided design such that they are focused at the target when the leaf is fully open, fully closed, and at the beam center, with